https://doi.org/10.5194/egusphere-2025-4954
Preprint. Discussion started: 6 November 2025


# Correction and Calibration Protocol for Isotope Data via CRDS: A Study Case for $N_2O$ and Other Isotope Systems

Julius C. Havsteen[1*], Mehr Fatima[2*], Simone Brunamonti[1], Andrea Pogány[3], Thomas Hausmaninger[2], Benjamin Wolf[4], Reinhard Well[5], Joachim Mohn[1]

[1]Empa, Laboratory for Air Pollution / Environmental Technology, Dübendorf, Switzerland
[2]VTT Technical Research Centre of Finland Ltd, Espoo, Finland
[3]Physikalisch-Technische Bundesanstalt, Braunschweig, Germany
[4]Karlsruhe Institute of Technology (KIT), Institute of Meteorology and Climate Research, Atmospheric Environmental Research (IMK-IFU), Garmisch-Partenkirchen, Germany
[5]Thünen Institute of Climate-Smart Agriculture, Braunschweig, Germany

*Correspondence to*: Julius C. Havsteen (julius.havsteen@empa.ch), Joachim Mohn (joachim.mohn@empa.ch)
* These authors contributed equally to this work

**Abstract.** Advances in laser spectroscopy have significantly simplified the measurement of $N_2O$ isotopologues ($^{14}N^{15}N^{16}O$, $^{15}N^{14}N^{16}O$, $^{14}N^{14}N^{18}O$), but the raw data require extensive post-processing. This problem arises from the complexity of spectral fitting, which is controlled by an intricate interplay between the physics of vibrational spectroscopy, gas composition, fitting algorithm, and instrumental parameters. Following the general principles of identical treatment, the highest precision and accuracy is achieved when reference gases mimic the sample composition, which underpins our correction and calibration protocol.

This study presents a comprehensive and detailed correction and calibration protocol to post-process $N_2O$ isotopic data, exemplified by data obtained from three commercial cavity ring-down spectroscopy (CRDS) analysers (G5131-*i*, Picarro Inc.). Experimental correction functions for delta values on changes in $N_2O$, $CH_4$, $CO_2$ and $O_2$ concentrations were determined for individual analysers to derive a mathematical framework, which was verified with spectral simulations. We confirm that the apparent δ-values scale inversely with the $N_2O$ concentration, with the slope being analyser-specific and highly variable over short time intervals. Consequently, any instrument must be routinely characterised to maintain high-quality data. Furthermore, when $CH_4$ and $CO_2$ concentrations vary simultaneously, their combined spectral interference displays a non-additive interaction. We strongly advise removing $CO_2$ from the sample gas before analysis to ensure optimal data quality unless $CH_4$ / $CO_2$ variations are very small such as for $N_2O$ emissions from upland soils).

We provide an end-to-end, stand-alone MATLAB application with a user-friendly interface for standardised data reduction, which was validated by analysis of several known target gases but with different gas compositions. This protocol/MATLAB application aims to support researchers in efficiently obtaining high-quality and reliable $N_2O$ isotope data from the tested CRDS analyser model, while also providing a study case for data correction for other analyser models and detection schemes. Therefore, the code can be readily adapted to any isotope system for routine application.

https://doi.org/10.5194/egusphere-2025-4954
Preprint. Discussion started: 6 November 2025


## 1 Introduction

Nitrous oxide is a powerful greenhouse gas with a global warming potential about 300 times that of $CO_2$, and plays a significant role in stratospheric ozone depletion (Forster et al., 2007). Given that atmospheric $N_2O$ concentrations have been increasing steadily from about 270 ppb before the Industrial Revolution to present atmospheric levels of approximately 337.6 ppb (NOAA/GML; Lan et al., 2024), it becomes critically important to understand the underlying sources and sinks in the nitrogen cycle in order to tackle climate change. In this regard, the relative abundance of nitrous oxide's singly substituted isotopic species serve as potent tracers for distinguishing between various biogeochemical soil processes that produce and consume $N_2O$, such as nitrification and denitrification (Toyoda et al., 2017; Yu et al., 2020). Information about these pathways deepens our understanding of $N_2O$ emissions, supports the development of process-based biogeochemical models (Denk et al., 2019) and provides guidance to identify critical parameters controlling emissions (Gruber et al., 2022).

$N_2O$ is a linear asymmetric molecule (NNO). Its main isotopic species is $^{14}N^{14}N^{16}O$ and its most abundant isotopologues are $^{14}N^{15}N^{16}O$, $^{15}N^{14}N^{16}O$ and $^{14}N^{14}N^{18}O$ (Toyoda and Yoshida, 1999). The terms $^{15}N^{\alpha}$-$N_2O$ and $^{15}N^{\beta}$-$N_2O$ refer to the isotopologues with $^{15}N$ in the central (α) or terminal (β) position of the $N_2O$ molecule. Isotopic abundances are reported in the δ-notation, where $\delta^{15}N = (R(^{15}N/^{14}N)_{sample}/R(^{15}N/^{14}N)_{reference})$ -1 denotes the relative difference in isotope ratio in per mil (‰) of the sample versus a reference material. While atmospheric $N_2$ (AIR-$N_2$) is the reference material for $^{15}N/^{14}N$, Vienna Standard Mean Ocean Water (VSMOW) is the international isotope-ratio scale for $^{18}O/^{16}O$. Using laser spectroscopy δ-values are calculated from measurement of isotopologue ratios of sample and reference gases, with the latter being defined on the AIR-$N_2$ and VSMOW scales (Mohn et al., 2022; Ostrom et al., 2018). By extension, $\delta^{15}N^{\alpha}$ denotes the corresponding relative difference of isotope ratios for $^{14}N^{15}N^{16}O/^{14}N^{14}N^{16}O$, and $\delta^{15}N^{\beta}$ for $^{15}N^{14}N^{16}O/^{14}N^{14}N^{16}O$. The site-specific intramolecular distribution of $^{15}N$ within the $N_2O$ molecule is termed $\delta^{15}N$ site preference ($\delta^{15}N^{SP}$) and is defined as $\delta^{15}N^{SP} = \delta^{15}N^{\alpha} - \delta^{15}N^{\beta}$. The term $\delta^{15}N^{bulk}$ is used to express the average $\delta^{15}N$ value and is equivalent to $\delta^{15}N^{bulk} = (\delta^{15}N^{\alpha} + \delta^{15}N^{\beta})/2$.

Advances in laser spectroscopy have enabled the precise measurement of $N_2O$ isotopologues even at ambient concentrations. It holds significant advantages relative to isotope ratio mass spectrometry (IRMS) in its ability to perform on-line analyses with little or no sample preparation. In addition, compact analysers have been commercialised for in-field applications, which are specific for intra-molecular $^{15}N$ substitution in the asymmetric $N_2O$ molecule. Despite its ease of use, the obtained data require extensive post-processing before the uncertainty of isotope deltas complies with set data quality objectives (Harris et al., 2020). This is due to the complex interplay between fundamental physical parameters, such as the temperature and pressure dependences of line intensity, width and position, with gas composition, i.e. concentrations of spectrally interfering substances and bulk gas constituents (gas matrix composition), as well as company-specific spectral fitting algorithms and instrumental settings. For retrieving accurate and comparable results, reference gases should closely mimic the sample gas composition following the identical treatment principle (Werner and Brand, 2001). Remaining deviations in gas composition between the reference and the sample gas should be eliminated or assessed for their effect on apparent delta values based on available

https://doi.org/10.5194/egusphere-2025-4954
Preprint. Discussion started: 6 November 2025


literature, manufacturer recommendations or laboratory tests. If significant effects are expected, analyser-specific correction functions should be established based on targeted experiments.

In this study, we developed a mathematical framework for correction of apparent $N_2O$ isotope delta values measured in ambient air with a commercial CRDS analyser (G5131-*i*, Picarro Inc.). Experimental correction functions for variations in $N_2O$, $CH_4$ and $CO_2$ concentrations were derived for three individual analyser specimen and dependencies confirmed by spectral simulations. In addition, we provide a stand-alone MATLAB software application with an intuitive user interface designed for standardised data reduction and post-processing, applying analyser-specific corrections. The post-processing algorithm was validated using a range of gas mixtures with known delta values but variable gas composition. With this extensive post-processing toolkit, we aim to enable researchers to efficiently acquire accurate $N_2O$ isotope data sets for CRDS analysers but also laser spectrometers with other detection schemes (direct absorption, off-axis integrated cavity output spectroscopy, etc.) or for other isotope systems. This protocol can contribute to developing and applying standardised community guidelines for post-processing isotope datasets, enabling consistency, reliability and enhanced inter-laboratory compatibility.

## 2 Materials and Methods

The focus of this study was the development and validation of a correction and calibration scheme, implemented in a MATLAB code, to retrieve accurate data from a commercial CRDS analyser for $N_2O$ isotopes (G5131-*i*, Picarro Inc., USA). A central part of the scheme are correction terms for $N_2O$ non-linearity and spectral interferences, with a focus on $CH_4$ and $CO_2$, shown to be critical for $N_2O$ soil flux applications. In addition, gas matrix effects, which are relevant for studies under reduced oxygen content, such as wastewater treatment, were tested. While the mathematical formalism for corrections has been described earlier (Wanlu et al., 2024; Braden-Behrens et al., 2023) it has not been realised for $N_2O$ isotope analysis by CRDS before. The suggested formalism for the G5131-*i* analyser is detailed in the Appendix (A1). Section 2.1 gives details on the applied analysers, their precision and benefits of drift correction. In section 2.2 procedures used for spectral simulation and calculation of delta values thereof are described. Section 2.3 provides information on experiments, while Section 2.4 gives details on data processing using the MATLAB code. To generalise observations and provide an in-depth understanding of mechanisms experimental results are compared to spectral simulations (Sections 2.2 and 3).

### 2.1 Cavity ring-down spectrometer (G5131-*i*)

Three CRDS analysers of the same model (G5131-*i*, Picarro Inc., USA) were used in this study for $N_2O$ concentration and isotopic analysis. The availability of three individual analysers, referred to as CRDS-I, CRDS-II and CRDS-III, in the same set of experiments facilitates the comparison of analyser specimen-specific correction functions to speculate on the possibility of generalised model-specific corrections. CRDS-I (serial number 5080-DAS-JDD S5089, year of production 2018) was provided by Empa (Dübendorf, Switzerland), CRDS-II (serial number 5056-PPU-JDD S5065, year of production 2017) was contributed by the Thünen Institute of Climate-Smart Agriculture (Braunschweig, Germany) and CRDS-III (serial number

https://doi.org/10.5194/egusphere-2025-4954
Preprint. Discussion started: 6 November 2025


5070-PVU-JDD S5079, year of production 2018) by the Karlsruhe Institute of Technology (Garmisch-Partenkirchen, Germany). CRDS-III was already applied in an earlier study (Harris et al., 2020) and therefore results can be compared to evaluate stability of correction terms on longer timescales. Aside the G5131-*i* model analysers, a G2401 gas concentration analyser (Picarro Inc., USA) for CO, $CO_2$, $CH_4$, and $H_2O$ was used to derive accurate trace gas concentrations in all experiments. Operational consistency of all three G5131-*i* instruments during the experimental period was not achieved, due to failure of individual analysers, which indicates challenges when working with this analyser model. The experimental period spanned from August 2023 to May 2025. Within this period, CRDS-I was operational from August 2023 till May 2024, whereafter it was sent for repair, while CRDS-II was operational from December 2023 throughout the rest of the experimental period. Lastly, CRDS-III was included in this study somewhat later to expand the dataset and confirm observed analyser-specific and universal corrections. It was operational at the interval from July 2024 until August 2024 and April 2025 to May 2025.

Allan-Werle experiments were conducted regularly throughout the entire experimental period to check the analyser status and assess optimal integration times for acquiring data with sufficient precision but also drift effects of the analysers over longer time intervals (Werle et al., 1993). These experiments were performed analysing pressurised ambient air (Cal $1.2_{330ppb}$; Table 1**)** over approximately 24 hours. From the acquired data, three different datasets were generated and subsequently evaluated using the Allan variance technique (Fig. 1), a standard method for assessing frequency stability over varying timescales (Werle et al., 1993; Barnes and Allan, 1966). The first dataset consisted of the raw, uncorrected analyser output, but binned to 15 s temporal resolution. To cover experiments in which distinct samples, such as bag samples, are analysed, the original dataset was segmented into consecutive 15-minute intervals, and these intervals were identified as alternating between reference and sample gas measurements. For each interval, the first 10 minutes were discarded, and the final 5 minutes were averaged. Based on this procedure, the second dataset consisted of those 5-minute averages identified as sample gas measurements, while for the third dataset the sample gas measurements were drift-corrected using the 5-minute averages identified as reference gas measurements. The latter approach is expected to provide superior performance as it involves intermittent drift correction as applied in replicate analysis of a sample. The Allan variance analysis indicates maximum precision (square root of the Allan variance) for CRDS-I and -II at 0.1 – 0.2 ‰, averaging up to 10'000 s ($10^4$ s), for CRDS-III somewhat lower, around 0.3 ‰, integrating measurement data for only 1'000 s ($10^3$ s). The Allan precision for the tested analysers was found to be superior to the manufacturer's specification at near ambient $N_2O$ concentrations, i.e. < 1.0 ‰ for $\delta^{15}N^{\alpha}$, $\delta^{15}N^{\beta}$ and $\delta^{18}O$, respectively (5 min averaging, ~330 ppb). 5-minute averaging and consideration of 10-minute stabilisation periods provide similar precision but at longer integration times. Drift correction is an efficient method for providing high-precision data for integration intervals that exceed the Allan minimum, which is particularly evident for CRDS-III. The Allan precision of the 5-minute averaged & drift corrected data shown in Fig. 1 was in the range of 0.2–0.8 ‰, similar to standard errors plotted in Figs. 5–8 for the respective CRDS systems.

https://doi.org/10.5194/egusphere-2025-4954
Preprint. Discussion started: 6 November 2025


**Table 1: $N_2O$, $CH_4$, $CO_2$ and CO concentrations and $N_2O$ isotopic compositions in reference gases used throughout this study. Matrix a is synthetic air: $N_2$ / $O_2$, matrix c is full synthetic air: $N_2$ / $O_2$ / Ar / $CO_2$ / $CH_4$ / CO. More details on the composition are given in Table 3. Provided uncertainties are specified in the subscript.**

| Name | Matrix | $N_2O$ (ppb) | $\delta^{15}N^{\alpha}$ (‰) | $\delta^{15}N^{\beta}$ (‰) | $\delta^{18}O$ (‰) | $CH_4$ (ppb) | $CO_2$ (ppm) | CO (ppb) |
|---|---|---|---|---|---|---|---|---|
| High-concentration reference gases [1)] | | | | | | | | |
| *Cal* $1_{90ppm}$ | Matrix a | ~ 92 200 | 2.06 ± 0.05 | 1.98 ± 0.20 | 36.12 ± 0.32 | <0.25 | <0.1 | <0.200 |
| *Cal* $2_{90ppm}$ | Matrix a | ~ 90 000 | -82.14 ± 0.49 | -78.02 ± 0.08 | 21.64 ± 0.12 | <0.25 | <0.1 | <0.200 |
| *Reference gases for static vs dynamic dilution experiment* [2)] | | | | | | | | |
| *RM-1-1*$_{pure}$ | $N_2O$ | $1\times10^9$ | -0.22 ± 0.46 | 0.82 ± 0.46 | 39.22 ± 0.15 | n.a. | n.a. | n.a. |
| *RM-1-1*$_{Diluted-1}$ | Matrix c | 327.45 ± 0.03 | -0.22 ± 0.46 | 0.82 ± 0.46 | 39.22 ± 0.15 | 2021.54 ± 0.16 | 399.98 ± 0.02 | 207.17 ± 1.04 |
| *RM-1-1*$_{Diluted-2}$ | Matrix c | 327.54 ± 0.03 | -0.22 ± 0.46 | 0.82 ± 0.46 | 39.22 ± 0.15 | 2019.27 ± 0.16 | 399.25 ± 0.02 | 204.71 ± 1.53 |
| *Ambient concentration reference gases* [3)] | | | | | | | | |
| *Cal 1.1*$_{330ppb}$ | Matrix c | 326.47 ± 0.05 | 15.70 ± 0.31 | -3.21 ± 0.11 | 35.16 ± 0.35 | 1987.54 ± 0.11 | 392.28 ± 0.04 | 192.40 ± 0.17 |
| *Cal 1.2*$_{330ppb}$ | Matrix c | 329.08 ± 0.06 | 15.62 ± 0.34 | -3.07 ± 0.39 | 43.92 ± 0.11 | 2112.47 ± 0.20 | 437.30 ± 0.05 | 214.56 ± 0.17 |
| *Cal 2.1*$_{330ppb}$ | Matrix c | 328.31 ± 0.03 | -24.35 ± 0.32 | -22.94 ± 0.03 | 31.79 ± 0.12 | 1995.36 ± 0.11 | 393.81 ± 0.01 | 193.24 ± 0.23 |

n.a. not analysed

[1)] $N_2O$ isotopic analysis performed by Sakae Toyoda (Institute of Science Tokyo); indicated uncertainties are standard errors for replicate analysis, but do not enclose the uncertainty of standards applied for calibration.

[2)] $N_2O$ isotopic analysis of RM1-1 pure was performed as described in Mohn et al. (2022). Isotopic composition of diluted standards assumed to be identical to RM1-$1_{pure}$, i.e. no isotopic fractionation. $N_2O$, $CH_4$, $CO_2$ and CO concentrations analysed by WCC-Empa against NOAA/ESRL/GMD standards. The indicated uncertainties are standard deviations for replicate analyses.

https://doi.org/10.5194/egusphere-2025-4954
Preprint. Discussion started: 6 November 2025


[3] $N_2O$ isotopic analysis of Cal 1.1 and Cal 2.1 performed by Sakae Toyoda (Institute of Science Tokyo); indicated uncertainties are standard errors for replicate analysis but do not enclose uncertainty of standards applied for calibration. Isotopic composition of diluted standards assumed to be identical, i.e. no isotopic fractionation.

[3] $N_2O$ isotopic analysis of Cal 1.2 $_{330ppb}$ performed at Empa against primary standards analysed by Science Tokyo; indicated uncertainties are standard deviations for replicate analyses. $N_2O$, $CH_4$, $CO_2$ and CO concentrations analysed by WCC-Empa against NOAA/ESRL/GMD standards. The indicated uncertainties are standard deviations for replicate analyses.

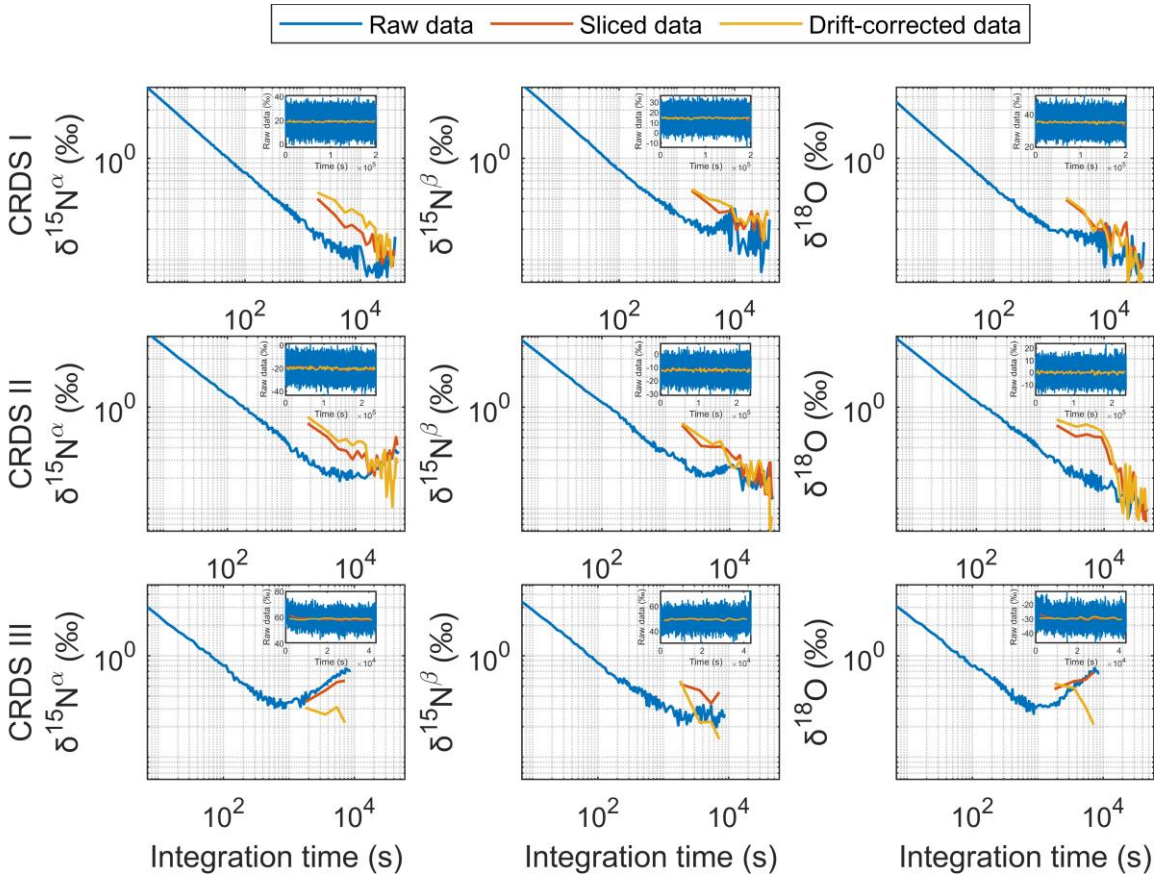


**Figure 1: Allan precision for the three tested CRDS analysers (CRDS I, II and III) analysing pressurised air (Cal 1.2$_{330\ ppb}$; Table 1). Three data sets are presented: Uncorrected raw data recorded at high temporal resolution binned to 15 s time intervals (blue), data averaged at 5-minute intervals (red) and drift-corrected 5-minute averaged intervals (yellow).**

https://doi.org/10.5194/egusphere-2025-4954
Preprint. Discussion started: 6 November 2025


## 2.2 Spectral simulations

Figure 2 shows a simulated spectrum for typical ambient concentrations of trace gases, i.e. 300 ppb $N_2O$, 400 ppm $CO_2$ and 2 ppm $CH_4$, together with a spectrum measured by the CRDS-I instrument in ambient air, both for the wavenumber window of 2195.7 to 2196.3 $cm^{-1}$, where the Picarro G5131-*i* spectrometer operates.

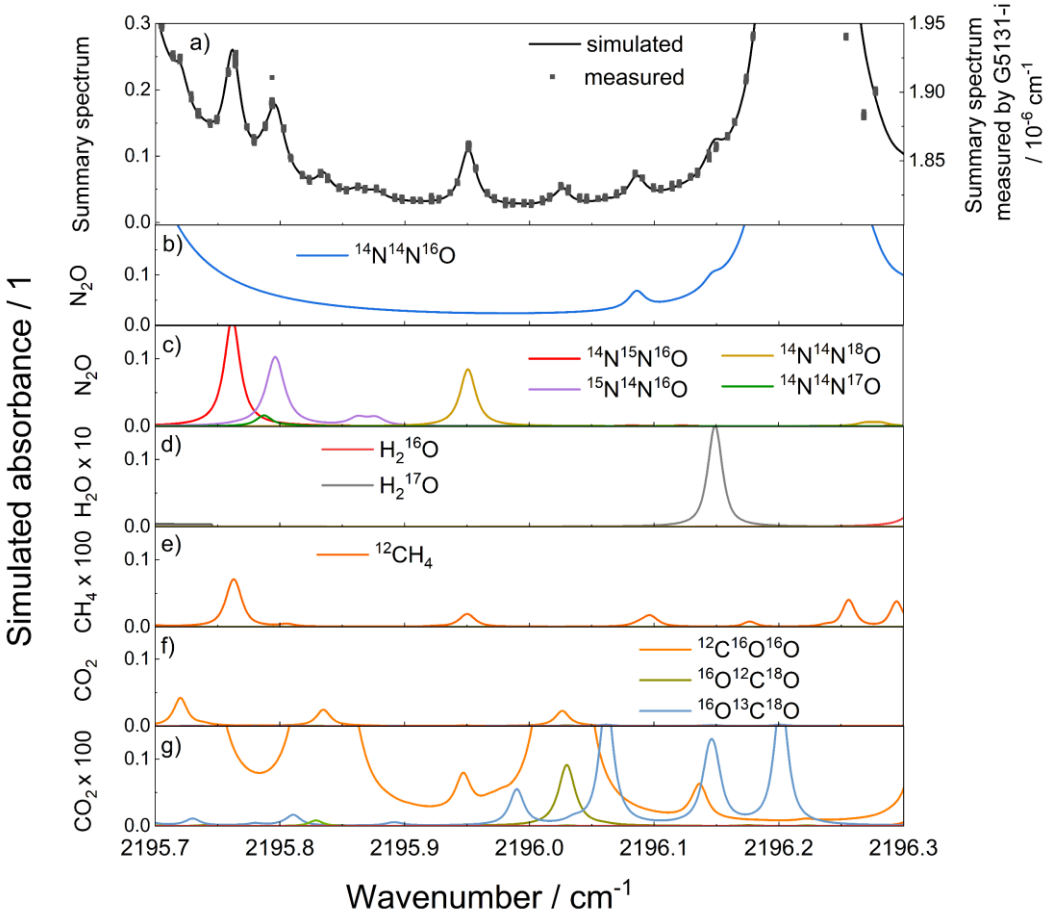


**Figure 2: Exemplary spectrum of ambient air measured with a G5131-*i* analyser (CRDS-I, black squares, right y-axis), compared to a simulated spectrum (top graph a, black line, left y-axis). The following molecules absorb in the wavelength region and are considered in the simulation: b) $N_2O$ main isotopologue ($^{14}N^{14}N^{16}O$, blue line); c) $^{14}N^{15}NO$ isotopologue ($^{15}N^{\alpha}$, red line), $^{15}N^{14}NO$ ($^{15}N^{\beta}$, violet line), $N_2{}^{18}O$ isotopic species (brown line), $N_2{}^{17}O$ isotopic species (green line); d) $H_2O$ 10x magnification: $H_2{}^{16}O$ (black line), $H_2{}^{17}O$ (grey line),; e) $CH_4$ 100x magnification (dark orange line) f) $^{13}CO_2$ (orange line), g) $CO_2$ 100 magnification: $^{13}CO_2$ (orange), $^{16}O^{12}C^{18}O$ (olive green) and $^{16}O^{13}C^{18}O$ (blue). Simulations were performed for 300 ppb $N_2O$, 400 ppm $CO_2$, 1% $H_2O$ and 2 ppm $CH_4$ in an ambient air matrix at 313 K, $10^4$ Pa and 20 km optical path length.**

Spectral simulations were performed using proprietary software written in LabVIEW. The software utilises spectral line data from the HITRAN2020 database (Gordon et al., 2022) to simulate the absorption spectrum, accounting for Doppler broadening of the spectral lines. In addition, pressure broadening by the matrix gas, pressure shift of the spectral lines as well as temperature

https://doi.org/10.5194/egusphere-2025-4954
Preprint. Discussion started: 6 November 2025


dependence of the line intensity and line broadening effects were considered. Spectra were simulated for the actual experimental conditions of 313 K gas temperature, 100 hPa gas pressure and 20 km absorption path length. The simulated spectra were fitted using a self-developed algorithm using the Fityk software (Wojdyr, 2010). While the simulations were performed using all spectral lines listed in the HITRAN 2020 database, in the fitting, we only considered those lines that have a measurable contribution to the spectrum within the spectral window of 2195.70–2196.3 $cm^{-1}$. The fitting approach followed the same principles as described in our recent publication (Pogány et al., 2025). The fitted lines included 19 $N_2O$ lines. Nine lines of the main $N_2O$ isotopic species were fitted as one line set, i.e. the relative line positions as well as ratios of the line intensities were calculated and used as fixed parameters in the fitting, together with Gauss and Lorentz line widths, leaving only the line area and position of the line at 2196.209 $cm^{-1}$ as free parameters. Three lines of the $^{15}N^{\alpha}$ isotopic species were fitted as a second line set, three lines of both the $^{15}N^{\beta}$ and the $^{14}N^{16}O^{17}O$ isotopologue as the third line set, and one $^{14}N^{16}O^{18}O$ line as a fourth line set. Furthermore, 12 $CO_2$ lines corresponding to different isotopic species were fitted as a fifth line set. In the line sets numbers 2–5, all line positions are given as fixed parameters relative to the position of the $N_2O$ line at 2195.209 $cm^{-1}$. The $CH_4$ lines are so weak compared to the $N_2O$ and $CO_2$ lines that they cannot be fitted independently; i.e., their influence on the spectrum cannot be considered in the fitting process.

Isotope ratios were calculated from the ratio of the line areas obtained from the spectral fitting, and the line intensities calculated for a temperature of 313 K, according to the following equation:

$$\delta = \left[\left(\frac{\alpha_i \cdot S_m}{\alpha_m \cdot S_i}\right) - \left(\frac{\alpha_i^{330} \cdot S_m}{\alpha_m^{330} \cdot S_i}\right)\right] \cdot 1000$$

where $\alpha_i$ is the line area (in $cm^{-2}$) and $S_i$ the line intensity (in $cm^{-1}$/(molecule x $cm^{-2}$)), for the minor, i.e. $^{15}N^{\alpha}$, $^{15}N^{\beta}$ or $^{14}N^{16}O^{18}O$ isotopic species, and $a_m$ the line area and $S_m$ the line intensity for the main $N_2O$ isotopologue. The superscript 330 corresponds to values determined from the spectrum simulated for a gas composition of 330 ppb $N_2O$ in synthetic air containing no $CO_2$ or $CH_4$, which we chose as a reference point for the delta values. Relative delta values were calculated as the difference between simulated results for the experimental conditions and reference conditions (330 ppb $N_2O$ in synthetic air), and compared to the experimental results.

https://doi.org/10.5194/egusphere-2025-4954
Preprint. Discussion started: 6 November 2025


### 2.3 Experimental design, laboratory setup, measurement procedures

#### 2.3.1 Experimental design

In Table 2 the main experiments conducted in this study are given. .

**Table 2: Overview table of conducted experiments. Matrix b is synthetic air with Ar ($N_2$ / $O_2$ / Ar), details on the composition are given in Table 3.**

| Experiment | Interference | $N_2O$ range | Interferant range | Gases used | Instruments used |
|---|---|---|---|---|---|
| Exp 1 (Sec. 3.1) $N_2O$ non-linearity | $N_2O$ effect on δ-values | 300 to 1200 ppb | n.a. | Cal-1, Cal-2, matrix b | CRDS-I, CRDS-II, CRDS-III |
| Exp 2 (Sec. 3.2) $CH_4$ Spectral Interference | $CH_4$ effect on δ-values | 330, 660, 990 ppb | $CH_4$: 0–10 ppm | Cal-1, Cal-2, matrix b, $CH_4$ in matrix b | CRDS-I, CRDS-II, CRDS-III |
| Exp 3 (Sec. 3.3) $CO_2$ Spectral Interference | $CO_2$ effect on δ-values | 330, 660, 990 ppb | $CO_2$: 0–2000 ppm | Cal-1, Cal-2, matrix b, $CO_2$ in matrix b | CRDS-I, CRDS-II |
| Exp 4 (Sec. 3.4) $O_2$ Matrix Gas Effects | $O_2$ effect on δ-values | 330, 660, 990 ppb | $O_2$: 12–21 % | Cal-1, Cal-2, matrix b, matrix d | CRDS-I, CRDS-II |
| Exp 5 (Sec. 3.5) Additivity Validation | $CH_4$ & $CO_2$ combined effects on δ-values | 330, 660 ppb | $CH_4$: 0–10 ppm & $CO_2$: 0–2000 ppm | Cal-1, Cal-2, matrix b, $CH_4$ in matrix b, $CO_2$ in matrix b | CRDS-II, CRDS-III |
| Exp 6 (Sec. S3) Dilution Validation | Static vs. dynamic dilution effects on δ-values | 330 ppb | n.a. | RM-1-1$_{Pure}$, RM-1-1$_{Diluted-1}$, RM-1-1$_{Diluted-2}$ | CRDS-II |

n.a. not analysed

#### 2.3.2 Laboratory setup

All experiments were conducted at the Laboratory for Air Pollution / Environmental Technology, Empa, Switzerland, in an air-conditioned laboratory maintained at 295 K (±1 K), with diel variation of ±0.5 K (Saveris 2, Testo AG, Switzerland).

https://doi.org/10.5194/egusphere-2025-4954
Preprint. Discussion started: 6 November 2025


Operation in an air-conditioned environment is not a must but supports superior data quality, as shown by Harris et al. (2020). The experiments were conducted using a calibration unit with seven mass flow controllers (MFC) with different flow ranges (2 x 25 mL $min^{-1}$, 100 mL $min^{-1}$, 2 x 500 mL $min^{-1}$, 1000 mL $min^{-1}$, 5000 mL $min^{-1}$, Vögtlin Instruments GmbH, Switzerland). Availability of MFCs with different flow ranges enabled the simultaneous mixing of $N_2O$ isotope reference gas with a target matrix or spectral interferant and a dilution gas in appropriate proportions to meet the target composition of a sample for a specific experiment. The selection of MFCs was tailored to each experiment in focus, such as investigating $N_2O$ non-linearity, $CH_4$ and $CO_2$ spectral interference, gas matrix effects or their combined impact. In a typical experiment, a highly concentrated reference gas (e.g., *Cal 1* $_{90ppm}$; *Cal 2* $_{90ppm}$; Table 1) was introduced through a low-flow range MFC channel (25 mL $min^{-1}$), a matrix or interferant test gas was dosed via a mid-range MFC channel (e.g., 100 mL $min^{-1}$) and a dilution gas (e.g., matrix b; Table 3) was added by a high-flow range MFC line (e.g., 1000 mL $min^{-1}$). The gases were combined in desired proportions with the dilution gas serving as a carrier gas to ensure homogenous mixing of the reference and target gases and short response times. This final gas mixture was then routed to the CRDS analysers using PTFE tubing. Additionally, the multi-position valve (MPV) information was electronically integrated into the experimental setup via CRDS-I/II, which controlled the Picarro Valve Sequencer software application. Figure 3 illustrates the general experimental setup, while Section S1 of the Supplementary Materials provide detailed information on individual experiments.

**Table 3: Concentrations of major constituents and trace gases in matrix and interference test gases used in this study.**

| Gas | Abbreviation | $O_2$ [1] (%) | Ar [1] (%) | $CO_2$ [2] (ppm) | $CH_4$ [2] (ppb) | CO [2] (ppb) | $N_2O$ [2] (ppb) |
|---|---|---|---|---|---|---|---|
| *Matrix gases* | | | | | | | |
| Synthetic air: $N_2$ / $O_2$ | Matrix a | 20.5 ± 0.5 | n.a | < 0.1 | < 0.25 | < 0.200 | < 0.25 |
| Synthetic air + Ar: $N_2$ / $O_2$ / Ar | Matrix b | 20.89 ± 0.2 | 0.90 ± 0.01 | < 0.5 | < 15 | < 150 | < 0.15 |
| Full synthetic air: $N_2$ /$O_2$ / Ar / $CO_2$ / $CH_4$ / CO | Matrix c | 20.95 ± 0.4 | 0.95 ± 0.02 | 397 ± 3 | 2004 ± 20 | 195 ± 3 | < 0.15 |
| Nitrogen: $N_2$ (5.0) | Matrix d | < 0.00003 | n.a. | n.a. | n.a. | n.a. | n.a. |
| | | $O_2$ [1] (%) | Ar [1] (%) | $CO_2$ [1] (%) | $CH_4$ [1] (ppm) | CO (ppb) | $N_2O$ (ppb) |
| *Interference test gases* | | | | | | | |
| $CO_2$ in synthetic air + Ar | $CO_2$ in matrix b | 21.06 ± 0.2 | 0.94 ± 0.01 | 4.02 ± 0.04 | n.a. | n.a. | n.a. |

https://doi.org/10.5194/egusphere-2025-4954
Preprint. Discussion started: 6 November 2025


| | | | | | | | |
|---|---|---|---|---|---|---|---|
| $CH_4$ in synthetic air + Ar | $CH_4$ in matrix b | 20.79 ± 0.4 | 0.96 ± 0.02 | n.a. | 199 ± 4 | n.a. | n.a. |

n.a. not analysed

1) Manufacturer specifications

2) Analysed by WCC-Empa against NOAA/ESRL/GMD standards. The indicated uncertainties are standard deviations for replicate analyses.

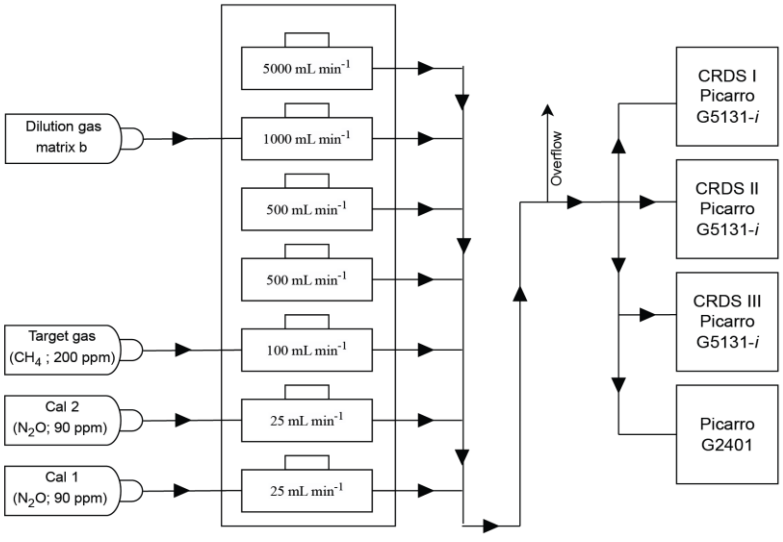


| *Parameter* | *Cal 1 / Cal 2* | *Sample 1* | *Sample 2* | *Sample 3* | *Sample 4* | *Sample 5* | *Sample 6* | *Sample 7* |
|---|---|---|---|---|---|---|---|---|
| Interferent test gas ($CH_4$ ppm) | 0 | 0.5 | 1 | 2 | 4 | 6 | 8 | 10 |
| Interferent test gas ($N_2O$ ppm) | 0.330 | 0.330 | 0.330 | 0.330 | 0.330 | 0.330 | 0.330 | 0.330 |
| Cal 1 / Cal 2 | 7.33 | 3.67 | 3.67 | 3.67 | 3.67 | 3.67 | 3.67 | 3.67 |
| Target Gas | 0.0 | 2.5 | 5 | 10 | 20 | 30 | 40 | 50 |
| Dilution Gas | 992.7 | 993.8 | 991.3 | 986.3 | 976.3 | 966.3 | 956.3 | 946.3 |
| Total flow | 1000 | 1000 | 1000 | 1000 | 1000 | 1000 | 1000 | 1000 |

*Each sample configuration was measured three times in three independent experiments.*

**Figure 3: Schematic illustration of the experimental setup used throughout this study in a configuration as applied for an exemplary experiment (Exp. 2, Section 3.2). For preparation of gas mixtures, a calibration unit that accommodates seven mass flow controllers (MFCs) was used. The setup allows flexible adjustment of gas flow rates and composition according to the specific requirements of each experiment. In the example shown, the unit was configured to deliver a steady concentration of 330 ppb $N_2O$ at various target concentrations of $CH_4$ between 0 and 10 ppm (see table above). While apparent $N_2O$ concentrations and isotopic composition were analysed with CRDS-I to -III, the actual interferant ($CH_4$, $CO_2$) concentration was determined with a G2401 analyser. Full details on the experimental setups and flow rates, are provided in the Supplementary Information (Section S1).**

### 2.3.3 Gas composition of $N_2O$ isotope reference gases and matrix as well as interferant test gases

Table 1 depicts the $N_2O$ mole fraction and associated isotopic compositions of reference gases used in this study. The mole fraction of $CH_4$, $CO_2$ and CO in the high-concentration $N_2O$ reference gases were acquired from the specification of their

https://doi.org/10.5194/egusphere-2025-4954
Preprint. Discussion started: 6 November 2025


matrix gases, while ambient concentration $N_2O$ reference gases were analysed for their trace gas composition at World Calibration Centre (WCC-Empa, Switzerland) of the World Meteorological Organization (WMO) Global Atmosphere Watch (GAW) program at Empa. WCC-Empa references measurements against reference standards acquired from the National Oceanic and Atmospheric Administration/Earth System Research Laboratory/Global Monitoring Division (NOAA/ESRL/GMD). $N_2O$ isotopic composition is referenced to international isotope ratio scales, Air-N2 for $^{15}N/^{14}N$ and VSMOW for $^{18}O/^{16}O$, and $\delta^{15}N^{SP}$, by analysis of high concentration standards at Institute of Science Tokyo (Cal $1_{90ppm}$, Cal $2_{90ppm}$, Cal 1.1, Cal 2.1) or several expert laboratories (RM 1-1 pure) as described in Mohn et al. (2022). For diluted standards (RM 1-$1_{Diluted-1}$, RM 1-$1_{Diluted-2}$, Cal $1.1_{330ppb}$, Cal $2.1_{330ppb}$), we assume identical isotopic composition to high concentration standards, within analytical uncertainties, which was confirmed as described in Supplementary Materials (Section S2).

Table 3 outlines the composition of matrix gases and interferant test gases for trace gas concentrations ($CH_4$, $CO_2$, CO) and major gas compounds ($O_2$, Ar, residual $N_2$). Four different matrix gases were applied: matrix a (synthetic air: $N_2$ / $O_2$), matrix b (synthetic air + Ar: $N_2$ / $O_2$ / Ar), matrix c (Full synthetic air: $N_2$ / $O_2$ / Ar / $CO_2$ / $CH_4$ / CO), matrix d ($N_2$). Matrix gases were analysed at WCC-Empa for the trace gases $CO_2$, $CH_4$, $H_2O$ (G1301, Picarro Inc., USA), and $N_2O$ as well as CO (LGR 913-0015-0000; Los Gatos Research Inc., USA). For all matrix gases, the concentration of $N_2O$ was below 0.25 ppb, but accurate detection of $N_2O$ and other trace gas concentrations in the interferant test gases was prevented by spectral interferences of high mole fractions of $CO_2$ or $CH_4$ on the respective optical analyser.

### 2.3.4 Measurements to quantify correction factors and for validation

Experiments for quantifying trace gas interferences, $N_2O$ non-linearity and $O_2$ matrix gas effects on apparent delta values and validation experiments are summarised in Table 2. The specific target gas concentrations and flows of $N_2O$ reference, matrix or interferant test and dilution gases used for each experiment are detailed in Supplementary Section S1. The experimental workflow consisted of three phases: an initial calibration phase (phase 1), an experimental phase, where apparent effects on delta values were characterised (phase 2), and a final calibration phase (phase 3). During phase 1 and 3, two reference gases (Cal $1_{90ppm}$ and Cal $2_{90ppm}$; Table 1), with different isotopic compositions, were diluted to ambient $N_2O$ concentrations and measured in triplicate. In phase 2, samples with constant $N_2O$ isotopic composition but differences in gas composition, e.g. concentration of $N_2O$, $CH_4$, $CO_2$, or $O_2$, were established by dynamic dilution of an $N_2O$ isotope reference gas (Cal $1_{90ppm}$). Sample analyses were bracketed by measurements of calibration gas 1 (Cal $1_{90ppm}$) diluted to ambient concentration, but without variation in the interferant, and instrumental drift was corrected using the two nearest Cal 1 measurements. Both sample and reference gases were measured for 15 minutes per analysis, which was chosen as a compromise between increased precision for longer averaging times and efficiency for gas consumption and workload. The last five minutes of the 15-minute sampling period were selected for further data processing. All experiments were conducted in triplicate on at least two or more calendar days. The analyser output data were processed, e.g. drift corrected and calibrated, with the MATLAB code described in Section 2.4.

https://doi.org/10.5194/egusphere-2025-4954
Preprint. Discussion started: 6 November 2025


Each data set was fitted using a linear fitting model in MATLAB to obtain the slope and intercept of the fit line. The standard error of the slope was calculated using the following formula:

$$SE(m) = \sqrt{\frac{1}{n-2}.\frac{\sum(y_i - \hat{y}_i)^2}{\sum\left(x_i - \underline{x_i}\right)^2}}$$

where; $y_i$ are the actual data points, $\hat{y}_i$ are the fitted values from the linear model, $x_i$ are the input values, $\underline{x_i}$ is the mean of $x$ values, and $n$ is the number of data points. The 95% confidence bounds are also marked for each fit. The goodness of fit from the model is represented by the adjusted coefficient of determination $R^2_{adj}$ value which, compared to the $R^2$ value also accounts for the number of predictors. The adjusted $R^2$ value is given by:

$$R^2_{adj} = 1 - \frac{(1 - R^2)(n-1)}{n-p-1}$$

where; $n$ is the number of data points, $p$ is the number of predictors (excluding the intercept), and $R^2$ is the coefficient of determination, which is measured as follows:

$$R^2 = 1 - \frac{SS_{res}}{SS_{tot}}$$

where; $SS_{res}$ is the residual sum of squares (sum of squared differences between observed and predicted values), and $SS_{tot}$ is the total sum of squares (sum of squared differences between observed values and their mean).

### 2.4 Data processing and MATLAB user application

We developed a customised MATLAB App for correction and calibration of experimental data. While our specific focus was $N_2O$ isotope analysis on ambient air samples with contributions from soil emissions, the approach can be adapted to any application with sequential analysis of gas samples, intermitted by reference gas analyses, such as bag analyses or on-line sampling from a laboratory or field setup.

The main functionalities of the code, outlined in Fig. 4, include: data import and pre-processing of $N_2O$ isotope data from a Picarro G5131-*i* analyser, as well as trace gas concentrations of, $CO_2$ and $CH_4$ from a supportive Picarro G2401 analyser, instrumental parameters check, correction and calibration of concentration data, and correction and calibration of $\delta$-values. All corrections are optional and can be individually activated by the user via a graphic user interface. In addition, the code can also provide a propagated uncertainty on the reported $\delta$-values. The approach used for the data treatment, correction and calibration is described below, while a full description of the mathematical model, including all equations, can be found in Appendix A1.

https://doi.org/10.5194/egusphere-2025-4954
Preprint. Discussion started: 6 November 2025


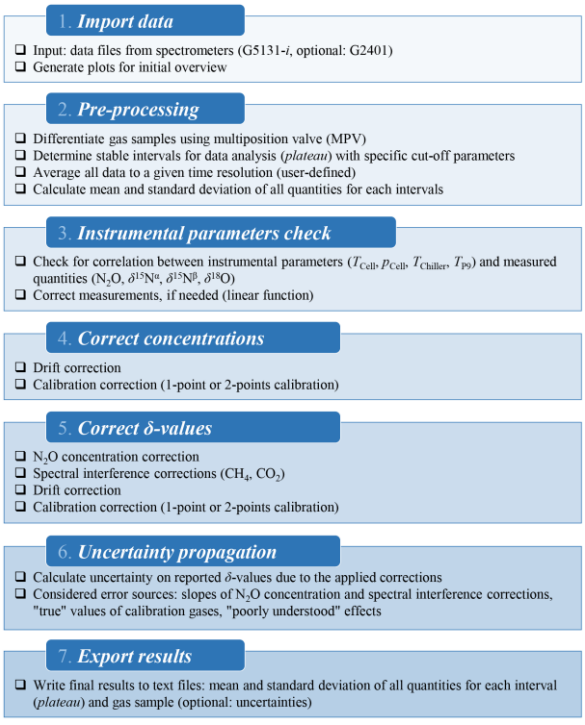


**Figure 4: Flowchart illustrating the data post-processing workflow, including data import, plateau identification, co-averaging, parameter-based and drift corrections, calibration, uncertainty assessment and final output. Individual corrections, e.g. for instrument parameters and the uncertainty propagation are optional. 2.4.1 Data import and pre-processing**

The output files of the G5131-*i* analyser, including $N_2O$ concentration and $\delta$-values of the three measured isotopologues ($\delta^{15}N^{\alpha}$, $\delta^{15}N^{\beta}$, $\delta^{18}O$), and the G2401 analyser, including concentrations of CO, $CO_2$ and $CH_4$, are used as input for the MATLAB code. After importing the data, measurement intervals are identified by sample or reference labels and the start/end time for each interval for data analysis (*plateau*) is defined. For the labelling of measurement intervals, the readout values of the multi-position valve (MPV, EMT-CSD10MWE, Vici AG, Switzerland) of the gas inlet and calibration unit are applied. The readout value of the MPV is used to track gas identity by assigning specific identification numbers to sample and calibration gases useful for post-processing the obtained data (see Section 2.3.2). The *plateau* intervals can be defined by either a fixed duration (e.g., 5 min) before the next switching of the valve position, or by constraining the stability (maximum standard deviation and range) of $N_2O$ concentration and pressure during the interval itself. An option is also provided to import a list of "gas type switch" times and labels from a generic text file, instead of using the output of the MPV (if this is not available). Finally, all data are integrated to a user-defined time resolution (e.g., 15 s), and mean and standard deviation of all quantities are calculated for each interval and gas type at the selected averaging time.

https://doi.org/10.5194/egusphere-2025-4954
Preprint. Discussion started: 6 November 2025


### 2.4.1 Instrumental parameters check

First, the data are checked for potential correlations of the measured quantities with instrumental parameters of the G5131-*i* analyser, including cell pressure ($p_{Cell}$), cell temperature ($T_{Cell}$), chiller temperature ($T_{Chiller}$), and P9 (i.e., back-mirror) temperature ($T_{P9}$). If a significant correlation is observed between either the $N_2O$ concentration or the $\delta$-values of the different isotopologues ($\delta^{15}N^{\alpha}$, $\delta^{15}N^{\beta}$, $\delta^{18}O$) and one of the instrumental parameters, the data can be corrected by a linear function (see Appendix A1, Eq. A5-A6). A "correlation matrix" plot of [$N_2O$] and all $\delta$-values against all instrumental parameters (showing also $R^2$ correlation coefficients) is generated by the code, allowing the user to easily identify anomalous correlations. The slope of the correction function is determined by a linear fit between the raw $N_2O$ concentration (or $\delta$-value) and the considered controlling parameter, recorded during measurements of reference gas 1 (*Cal* 1). The reason for choosing *Cal 1* measurements for this correction was that this gas is measured repetitively over the course of a day. The mean value of the controlling parameter during *Cal 1* measurements is used as a reference point, where no correction is applied.

### 2.4.2 Correction and calibration of $N_2O$ concentration

Before correcting the $\delta$-values, the measured concentrations of $N_2O$ (from G5131-*i*) and $CH_4$, CO and $CO_2$ (from G2401) are corrected for drift and calibrated. The *drift correction* considers instrumental drifts of measurement signals over time, which manifest by changes in $N_2O$, $CH_4$, CO and $CO_2$ concentrations during *Cal 1* measurements. For each sample interval, the "offset" due to drift is calculated as the difference between the linear interpolation of the two nearest (bracketing) *Cal 1* intervals and its mean value over all *Cal 1* intervals (Eq. A7-A8). Consequently, all *Cal 1* measurements are corrected to their mean value. Then, the data are calibrated by a one- or two-point *calibration correction* (Eq. A9-A10), depending on the number of available reference gas measurements for which the "true" concentration values are known. For a single calibration gas (*Cal 1*), this corresponds to the offset of all data by the difference between the mean of all *Cal 1* measurements and its "true" value.

### 2.4.3 Correction and calibration of $\delta$-values

The correction and calibration of the δ-values consists of four steps: $N_2O$ concentration correction, $CH_4$ and $CO_2$ spectral interference corrections, drift correction and calibration correction.

The $N_2O$ concentration correction considers the apparent dependencies of the isotopic readings ($\delta^{15}N^{\alpha}$, $\delta^{15}N^{\beta}$, $\delta^{18}O$) of the analyser on the $N_2O$ concentration. Based on observations from three analysers, the $N_2O$ concentration dependency is assumed to be proportional to the inverse of the $N_2O$ concentration (i.e., 1/[$N_2O$]) (see Appendix A1, Eq. A12). Importantly, the slope of the correction line (to be defined by the user) is analyser-specific and must be experimentally quantified for any specific analyser by means of a dedicated experiment with varying $N_2O$ concentration at constant isotopic composition (as done in this work). The mean $N_2O$ concentration of Cal 1 is used as a reference point, where no correction is applied.

The spectral interference corrections (for $CH_4$, $CO_2$) consider spectral interference effects by neighbouring $CH_4$ and $CO_2$ absorption lines on the $\delta^{15}N^{\alpha}$, $\delta^{15}N^{\beta}$, and $\delta^{18}O$ retrievals of G5131-i. These effects have been shown to be proportional to the

https://doi.org/10.5194/egusphere-2025-4954
Preprint. Discussion started: 6 November 2025


[$CH_4$]/[$N_2O$] and [$CO_2$]/[$N_2O$] ratios, respectively (Harris et al., 2020) (Appendix A1, Eq. A12-A14). Again, the slope of the correction line is user-defined and must be experimentally quantified by means of dedicated experiments with varying $CH_4$ and $CO_2$ concentrations at constant isotopic composition. The mean $CH_4$ and $CO_2$ concentrations of Cal 1 are used as reference points, where no correction is applied.

Then, a drift correction is applied to all δ-values, calculated as for the concentration corrections (see Eq. A15), and finally the δ-values are calibrated by a one- or two-point calibration correction (Eq. A16-A17). The calibration function is calculated based on the measured and the "true" values of $\delta^{15}N^{\alpha}$, $\delta^{15}N^{\beta}$, and $\delta^{18}O$ of Cal 1 (1-point calibration, i.e. offset), or both Cal 1 and reference gas 2 (Cal 2), if available (2-point calibration).

#### 2.4.4 Uncertainty propagation and data export

The established MATLAB code has the potential to optionally calculate a propagated uncertainty for the reported *δ*-values. For this, the law of error propagation (Jcgm, 2008), exemplified for $CH_4$ isotopic species in Sperlich (2024) was applied to the mathematical framework used to calculate the *δ*-values.. The considered error sources include uncertainties in the slopes applied for the $N_2O$ concentration correction, the spectral interference corrections, uncertainties in the *δ*-values attributed to reference gases, and uncertainties due to poorly understood effects, which were approximated by repeatability for target gas measurements. The equations used for error propagation, including individual derivatives of the measurement model for each error term, are presented in Appendix 1 (Eqs. A18-A28). While the functionality of the uncertainty propagation was implemented in the MATLAB algorithm for future use, it was not tested in this study.

After all corrections have been applied, the results can be exported as ASCII (text) files, including the mean and standard deviation of all quantities for each measurement interval (*plateau*) and sample gas, plus optionally, the propagated uncertainty, comprising all relevant contributions. In addition, a "logfile" text file is generated, documenting information on every applied correction and its corresponding input parameters.

## 3. Results

In the following sections, the apparent δ-values of $N_2O$ for the tested G5131-*i* analysers under changing $N_2O$, $CH_4$, $CO_2$ and $O_2$ concentrations (Sections 3.1–3.4) are provided. The determined regression slopes or interference coefficients, $m_{N2O}$, $m_{CO2}$, $m_{CH4}$ and $m_{O2}$ , for all experiments are given in Table 4–7 and are used to parametrise the MATLAB algorithm. To confirm mathematical corrections and provide insights into spectral analysis and data post-processing of the analysers, the simulated interference coefficients are given for comparison. In a next step, the additivity of $N_2O$, $CH_4$ and $CO_2$ concentration effects is tested in a validation study (Section 3.5).

https://doi.org/10.5194/egusphere-2025-4954
Preprint. Discussion started: 6 November 2025


355

### 3.1 $N_2O$ non-linearity (Exp. 1)

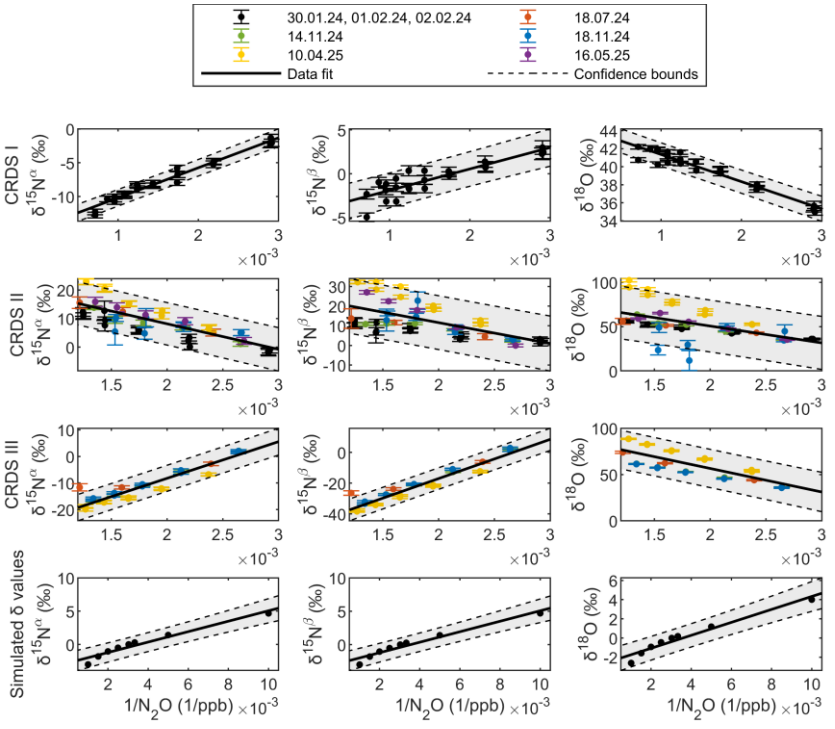


360 **Figure 5: Apparent changes in $N_2O$ isotopic composition versus 1/$N_2O$. In the top three rows, experimental data for three CRDS analysers (CRDS I, CRDS II and CRDS III) are provided. The coloured points represent the data sets measured on different days. For CRDS I, the data points are combined into a single cluster (black symbols), since they were measured over only four days. Each data point presents an average of 5 minutes of sample measurement. The error bars represent the standard errors, calculated by incorporating the standard deviations from both the sample measurements and the neighbouring calibration gas measurements.**
365 **The regression line is plotted in black (slope is $m_{N2O}$), corresponding to the combined coefficient in Table 4, while the black shaded area shows the 95% confidence bounds of this fit. The bottom row shows the simulated delta values plotted as a function of 1/$N_2O$.**

Although the three tested CRDS analysers are the same analyser model, they offer different $N_2O$ operation ranges, i.e. CRDS-II and -III displayed increasing data loss already above ~700–800 ppb $N_2O$, which most probably is related to enhanced absorption of the empty cavity(e.g. by dust particles) and therefore partial saturation of the absorption features at higher $N_2O$
370 concentrations. Therefore, only CRDS-I was tested in between 330 and 1200 ppb $N_2O$, while CRDS-II and -III were only operated up to 800 ppb $N_2O$. Figure 5 provides dependencies of apparent δ-values of $N_2O$ isotopologues ($\Delta\delta^{15}N^{\alpha}$, $\Delta\delta^{15}N^{\beta}$, $\Delta\delta^{18}O$) on inverse $N_2O$ concentrations for all three G5131-*i* analysers as well as for simulated results. The experimentally determined regression slopes $m_{N2O}$ are applied to parametrise the developed MATLAB algorithm. Consistency of apparent δ-values from triplicate analyses for individual analysers confirms reproducible offsets, within short timeframes, between
375 measured and true δ-values for $N_2O$ concentration changes between sample and calibration gases (Fig. 5). A linear relationship

https://doi.org/10.5194/egusphere-2025-4954
Preprint. Discussion started: 6 November 2025


between apparent delta values and the inverse $N_2O$ concentration has already been observed by Harris et al. (2020). A closer look at the results of spectral simulations displays a slightly non-linear behaviour of the apparent isotope effect. For the experimental data, this effect is masked by instrumental precision, and therefore a linear correction was applied.

Clearly, the different analyser specimen (CRDS-I, CRDS-II, CRDS-III) and simulated results show contrasting regression slopes ($m_{N2O}$) (Table 4). Repetitive tests of individual analysers over longer timescales, such as several weeks or months, indicate that the $N_2O$ non-linearity correction is not only analyser-specific but also variable over time. CRDS-III tested here was already included in an earlier study (CRDS II in Harris et al. (2020)), but with substantially different non-linearity behaviour. Similarly, dependencies of delta values on $N_2O$ concentration changed significantly for CRDS-II, which was tested several times. The situation is complicated by the fact that the analyser software has a built-in post-correction to minimise $N_2O$ non-linearities, which is parametrised analyser-specific by Picarro Inc.

**Table 4: Experimentally derived correction functions for $N_2O$ non-linearity of CRDS analysers and spectral simulations. The correction slope $m_{N2O}$ is given in ‰ ppb, the intercept in ‰.**

| Analyser | Date | $\delta^{15}N^{\alpha}$ | | | $\delta^{15}N^{\beta}$ | | | $\delta^{18}O$ | | |
|---|---|---|---|---|---|---|---|---|---|---|
| | | Slope | Intercept | Adj. $R^2$ | Slope | Intercept | Adj. $R^2$ | Slope | Intercept | Adj. $R^2$ |
| CRDS-I | 30.01.24<br>01.02.24<br>02.02.24 | 4441 ± 175 | -14.62 | 0.97 | 2443 ± 282 | 4.34 | 0.76 | -3015 ± 184 | 44.37 | 0.92 |
| CRDS-II | 30.01.24,<br>01.02.24,<br>02.02.24 | -8059 ± 697 | 20.97 | 0.90 | -5311± 758 | 17.15 | 0.77 | -11822 ± 512 | 70.11 | 0.97 |
| | 18.07.24 | -8784 ± 205 | 26.34 | 1.00 | -7900 ± 853 | 23.71 | 0.98 | -10703 ± 336 | 68.83 | 1.00 |
| | 14.11.24,<br>18.11.24 (2x) | -7387 ± 827 | 21.68 | 0.84 | -9360 ± 1298 | 28.70 | 0.77 | -11898 ± 4599 | 64.30 | 0.28 |
| | 10.04.25 (2x) | -12221 ± 759 | 37.01 | 0.96 | -17516 ± 1074 | 54.88 | 0.96 | -34569 ± 2236 | 137.61 | 0.96 |
| | 16.05.25 (1x) | -9958 ± 692 | 29.50 | 0.98 | -20441 ± 710 | 54.42 | 0.99 | -20725 ± 3999 | 92.18 | 0.86 |
| CRDS-II | Combined coef. ($m_{N2O}$) | -8939 ± 792 | 26.03 | 0.72 | -10632 ± 1458 | 32.85 | 0.51 | -19008 ± 3116 | 88.72 | 0.42 |
| CRDS-III | 18.07.24 | 8078 ± 2697 | -22.72 | 0.80 | 17984 ± 3710 | -50.03 | 0.92 | -25002 ± 1953 | 103.44 | 0.99 |
| | 14.11.24,<br>18.11.24 (2x) | 14884 ± 194 | -36.92 | 1.00 | 26739 ± 248 | -68.81 | 1.00 | -19044 ± 173 | 86.73 | 1.00 |
| | 10.04.25 (2x) | 11484 ± 281 | -33.87 | 0.99 | 22548 ± 264 | 66.09 | 1.00 | -30279 ± 415 | 126.67 | 1.00 |
| CRDS-III | Combined coef. ($m_{N2O}$) | 13811 ± 532 | -35.86 | 0.95 | 25511 ± 761 | -68.05 | 0.97 | -25428 ± 2241 | 107.40 | 0.77 |
| CRDS-III | (Harris et al. 2020) | 1313 | -4.52 | | -458 | 1.18 | | 962 | -3.23 | |
| Spectral simulations (330 – 1200 ppb) | | 784 ± 72 | -2.78 | 0.94 | 785 ± 70 | -2.79 | 0.95 | 675 ± 61 | -2.42 | 0.94 |

https://doi.org/10.5194/egusphere-2025-4954
Preprint. Discussion started: 6 November 2025


### 3.2 $CH_4$ spectral interference (Exp. 2)

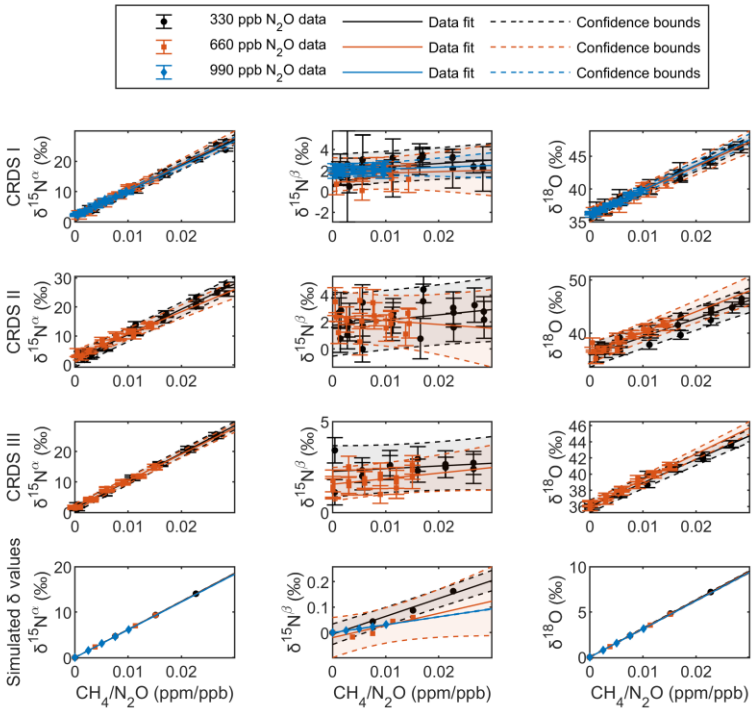


**Figure 6: Apparent changes in $N_2O$ isotopic composition versus $CH_4/N_2O$ for three CRDS analysers (top three rows CRDS-I, II and III) as well as spectral simulations (bottom row). The experimental data points for varying $CH_4$ concentration but at a constant $N_2O$ concentration are shown with different colour coding, black (330 ppb), orange (660 ppb) and blue (990 ppb), respectively. Each data point corresponds to the mean of three replicate measurements, where each replicate represents an average over 5 minutes. The error bars represent the standard errors, calculated by incorporating the standard deviations from both the sample measurements and the neighbouring calibration gas measurements. The regression lines for individual $N_2O$ concentrations are plotted in black (330 ppb), orange (660 ppb) and blue (990 ppb), while shaded areas show the 95% confidence bounds of the corresponding fits.**

Figure 6 shows the effect of $CH_4$ concentration changes, between 0 and 10 ppm, on apparent $N_2O$ delta values ($\Delta\delta^{15}N^{\alpha}$, $\Delta\delta^{15}N^{\beta}$, $\Delta\delta^{18}O$) for three different $N_2O$ concentrations (330, 660 and 990 ppb). Delta values display a linear relationship on $CH_4/N_2O$ concentration ratios, i.e., the interference effect doubles for samples with either a twofold $CH_4$ concentration or halving the $N_2O$ concentration. Dependencies of apparent delta values on $CH_4$ concentrations are most substantial for $\delta^{15}N^{\alpha}$, intermediate for $\delta^{18}O$ and weakest for $\delta^{15}N^{\beta}$ (Table 5). Results are generally consistent for repeated experiments (n = 3) and between analyser specimens (CRDS I, CRDS II, CRDS-III) as well as with literature data (Harris et al., 2020), which indicates that corrections might be specific for this particular CRDS analyser model (G5131-*i*) and constant over time. For analysers CRDS-II and CRDS-III, the upper $N_2O$ concentration limit for obtaining precise measurement data is 800 ppb due to enhanced background signals (see 3.1); therefore, experimental data obtained at 990 ppb were excluded from data analysis. Our spectral simulations

https://doi.org/10.5194/egusphere-2025-4954
Preprint. Discussion started: 6 November 2025


underpin the experimental results, although correction slopes for $\delta^{15}N^{\alpha}$ are significantly smaller compared to experimental results (Table 5).

The strong spectral interference, observed for $\delta^{15}N^{\alpha}$, can be explained by two $CH_4$ spectral lines at 2195.762 $cm^{-1}$ and 2195.764 $cm^{-1}$, with line intensities of 1.02 x $10^{-24}$ $cm^{-1}$ and 4.49 x $10^{-25}$ $cm^{-1}$, respectively (see Fig. 2). The spectral interference on $\delta^{18}O$ is a factor of two (for simulations) to three (for experimental results) weaker and caused by a single $CH_4$ line at 2195.95 $cm^{-1}$ with a line intensity of 4.26 x $10^{-25}$ $cm^{-1}$, overlapping with the $N_2{}^{18}O$ line. In the case of the $^{15}N^{\beta}$ isotopologue, the overlapping $CH_4$ line is approximately an order of magnitude weaker with a line intensity of 5.148 x $10^{-26}$ $cm^{-1}$; thus, the observed spectral interference and its effect on the δ-values are negligible. The main analytical challenge with respect to the $CH_4$ interference is the fact, that all $CH_4$ lines co-evolve with $N_2O$ lines, so no specific $CH_4$ concentration analysis is feasible within the wavelength region implemented in the G5131-*i* analyser. Therefore, the most straightforward approach is an empirical post-correction using an independent $CH_4$ concentration analyser, as suggested and implemented in this manuscript.

**Table 5: Experimentally derived correction functions for $CH_4$ spectral interference of CRDS analysers and simulated results. The correction slope $m_{NCH4}$ is given in ‰ [ppb $N_2O$] [ppm $CH_4$]$^{-1}$, the intercept in ‰.**

| Analyser | Date | $\delta^{15}N^{\alpha}$ | | | $\delta^{15}N^{\beta}$ | | | $\delta^{18}O$ | | |
|---|---|---|---|---|---|---|---|---|---|---|
| | | Slope | Intercept | Adj. $R^2$ | Slope | Interce pt | Adj. $R^2$ | Slope | Interce pt | Adj. $R^2$ |
| CRDS-I 330 ppb | 05.02.24 06.02.24 08.02.24 | 842 ± 17 | 1.84 | 0.99 | 32.49 ± 16.1 | 2.0 | 0.13 | 362 ± 8.1 | 36.20 | 0.99 |
| 660 ppb | 28.03.24 29.02.24 (2x) | 864 ± 34 | 1.86 | 0.98 | 13.91 ± 38.5 | 1.60 | -0.06 | 369 ± 26.4 | 36.07 | 0.93 |
| 990 ppb | 03.04.24 03.06.24 (2x) | 818 ± 22 | 2.08 | 0.99 | 17.39 ± 19.5 | 1.95 | -0.01 | 383 ± 14.1 | 36.01 | 0.97 |
| CRDS-I | Combined coef. | 838 ± 10 | 1.97 | 0.99 | 36.12 ± 10.8 | 1.78 | 0.15 | 367 ± 6.1 | 36.1 | 0.99 |
| CRDS-II 330 ppb | 05.02.24, 06.02.24, 08.02.24 | 876 ± 26 | 1.69 | 0.98 | 38.75 ± 23.63 | 1.75 | 0.08 | 343 ± 23 | 35.89 | 0.92 |
| 660 ppb | 28.03.24, 29.02.24 (2x), | 766 ± 47 | 3.02 | 0.94 | 28.29 ± 44.8 | 2.38 | -0.04 | 388 ± 42 | 36.28 | 0.84 |
| CRDS-II | Combined coef. | 848 ± 21 | 2.21 | 0.98 | 26.11 ± 18.8 | 1.95 | 0.02 | 334.36 ± 19 | 36.29 | 0.89 |
| CRDS-III 330 ppb | 05.02.24 06.02.24 08.02.24 | 902 ± 17 | 1.35 | 1.00 | 14.91 ± 18.2 | 2.26 | -0.03 | 290 ± 10 | 36.02 | 0.99 |
| 660 ppb | 28.03.24 29.02.24 (2x) | 860 ± 21 | 1.87 | 0.99 | 30.54 ± 18.5 | 1.56 | 0.09 | 320 ± 12 | 36.11 | 0.98 |
| CRDS-III | Combined coef. | 885 ± 12 | 1.64 | 0.99 | 34.20 ± 12.8 | 1.72 | 0.17 | 290 ± 8 | 36.21 | 0.98 |
| CRDS-III | (Harris et al. 2020) | 822[1)] | | | 27.95[1)] | | | 426[1)] | | |
| Simulated coefficients 330 ppb | | 618 ± 0.4 | 0 | 1 | 7.02 ± 0.4 | -0.01 | 0.99 | 317 ± 0.6 | 0 | 1 |
| 660 ppb | | 614 ± 0.3 | 0 | 1 | 4.77 ± 1.6 | -0.02 | 0.65 | 313 ± 0.9 | -0.01 | 1 |
| 990 ppb | | 612 ± 0.4 | 0 | 1 | 3.12 ± 0.0 | 0 | 1 | 312 ± 0.0 | 0 | 1 |

[1)] Correction slopes were calculated from regression functions given in Fig. S4–7 of Harris et al. (2020) for 330 ppb $N_2O$.

https://doi.org/10.5194/egusphere-2025-4954
Preprint. Discussion started: 6 November 2025


### 3.3 $CO_2$ spectral interference (Exp. 3)

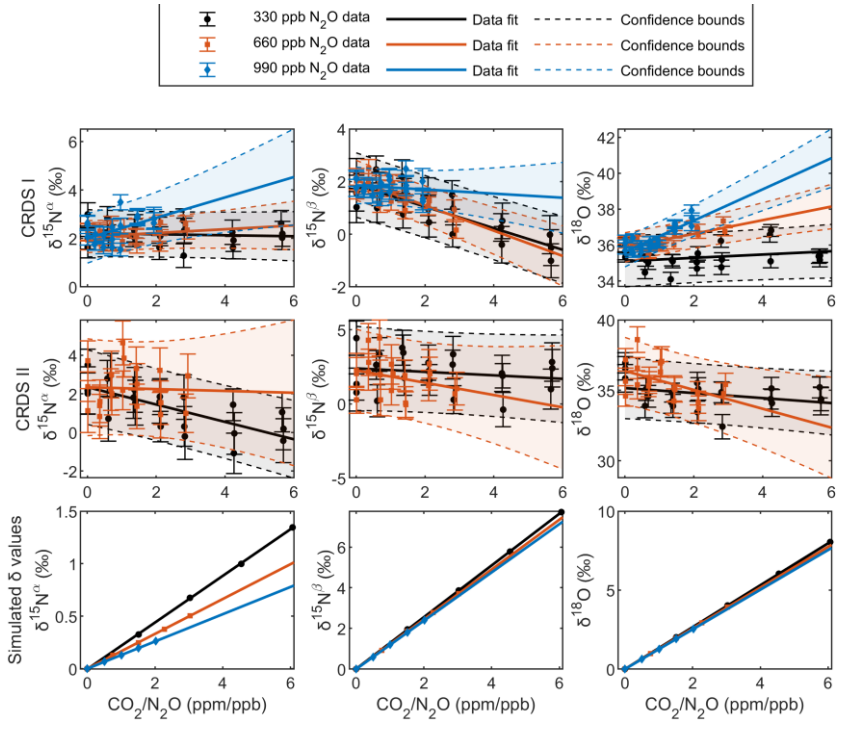


**Figure 7: Apparent changes in $N_2O$ isotopic composition versus $CO_2/N_2O$ for two CRDS analysers (top two rows, CRDS-I and II) as well as spectral simulations (bottom row). The experimental data points for varying $CO_2$ concentration but at a constant $N_2O$ concentration are shown with different colour coding, black (330 ppb), orange (660 ppb) and blue (990 ppb), respectively. Each data point corresponds to the mean of three replicate measurements, where each replicate represents an average over 5 minutes. The error bars represent the standard errors, calculated by incorporating the standard deviations from both the sample measurements and the neighbouring calibration gas measurements. The regression lines for individual $N_2O$ concentrations are plotted in black (330 ppb), orange (660 ppb) and blue (990 ppb), while shaded areas show the 95% confidence bounds of the corresponding fits.**

Figure 7 displays the effect of $CO_2$ concentration changes in the range 0 to 2000 ppm on apparent δ-values for experimental results (CRDS-I and II) and spectral simulations. Experiments were conducted for three different $N_2O$ concentrations, 330 ppb, 660 ppb and 990 ppb, with each experiment repeated three times. CRDS-II was not capable to analyse gas mixtures at 990 ppb due to enhanced background and saturation effects (3.1). Overall, no consistent and significant effect of $CO_2/N_2O$ concentration changes on apparent δ-values was observed for the two analyser specimen (Fig. 7; Table 6). These results are in agreement with observations made by Harris et al. (2020) and imply that the interfering $CO_2$ absorption lines are either well enough separated or the CRDS quantification algorithm is able to correct effects appropriately. In contrast, spectral simulations indicate a stronger, significant spectral interference of $CO_2$ concentrations on the apparent isotopic delta values for $\delta^{15}N^{\beta}$ and

https://doi.org/10.5194/egusphere-2025-4954
Preprint. Discussion started: 6 November 2025


$\delta^{18}O$, and a minor effect on $\delta^{15}N^{\alpha}$. Apparent effects of up to 8 ‰ for $\delta^{15}N^{\beta}$ and $\delta^{18}O$ values are most probably due to computational differences between the spectral simulation and the analyser's fitting software.

**Table 6: Experimentally derived correction functions for $CO_2$ spectral interference of CRDS analysers and simulated results. The correction slope $m_{CO2}$ is given in ‰ [ppb $N_2O$] [ppm $CO_2$]$^{-1}$, the intercept in ‰.**

| Analyser | Date | $\delta^{15}N^{\alpha}$ | | | $\delta^{15}N^{\beta}$ | | | $\delta^{18}O$ | | |
|---|---|---|---|---|---|---|---|---|---|---|
| | | Slope | Intercept | Adj. $R^2$ | Slope | Intercept | Adj. $R^2$ | Slope | Intercept | Adj. $R^2$ |
| CRDS-I 330 ppb | 08.03.24, 13.03.24 (2x) | -0.02 ± 0.1 | 2.21 | -0.04 | -0.41 ± 0.1 | 1.87 | 0.66 | 0.09 ± 0.1 | 35.10 | 0.02 |
| 660 ppb | 14.03.24 (3x) | 0.08 ± 0.1 | 2.07 | 0 | -0.48 ± 0.1 | 2.05 | 0.61 | 0.38 ± 0.1 | 35.87 | 0.45 |
| 990 ppb | 19.03.24 (2x), 24.03.24 | 0.42 ± 0.2 | 2.01 | 0.23 | -0.08 ± 0.1 | 1.85 | -0.02 | 0.87 ± 0.1 | 35.62 | 0.69 |
| CRDS-I | Combined coef. | 0.01 ± 0.0 | 2.22 | -0.02 | -0.43 ± 0.0 | 2.02 | 0.66 | 0.00 ± 0.1 | 35.98 | -0.02 |
| CRDS-II 330 ppb | 08.03.24, 13.03.24 (2x) | -0.45 ± 0.1 | 2.34 | 0.48 | -0.12 ± 0.1 | 2.40 | -0.02 | -0.18 ± 0.1 | 35.16 | 0.07 |
| 660 ppb | 14.03.24 (3x) | -0.05 ± 0.3 | 2.34 | -0.05 | -0.42 ± 0.3 | 2.26 | 0.04 | 0.67 ± 0.3 | 36.37 | 0.21 |
| CRDS-II | Combined coef. | -0.45 ± 0.1 | 2.56 | 0.32 | -0.10 ± 0.1 | 2.14 | -0.01 | -0.33 ± 0.1 | 35.75 | 0.19 |
| CRDS-III | (Harris et al. 2020) | -0.23[1)] | | | 0.02[1)] | | | -0.40[1)] | | |
| Simulated coefficients 330 ppb | | 0.22 ± 0 | 0 | 1 | 1.27 ± 0 | 0.01 | 1 | 1.33 ± 0 | 0 | 1 |
| 660 ppb | | 0.17 ± 0 | 0 | 1 | 1.22 ± 0 | 0 | 1 | 1.29 ± 0 | 0 | 1 |
| 990 ppb | | 0.13 ± 0 | 0 | 1 | 1.19 ± 0 | 0 | 1 | 1.26 ± 0 | 0 | 1 |

[1)] Correction slopes were calculated from regression functions given in Fig. S4–6 of Harris et al. (2020) for 330 ppb $N_2O$.

https://doi.org/10.5194/egusphere-2025-4954
Preprint. Discussion started: 6 November 2025


### 3.4 $O_2$ matrix gas effects (Exp. 4)

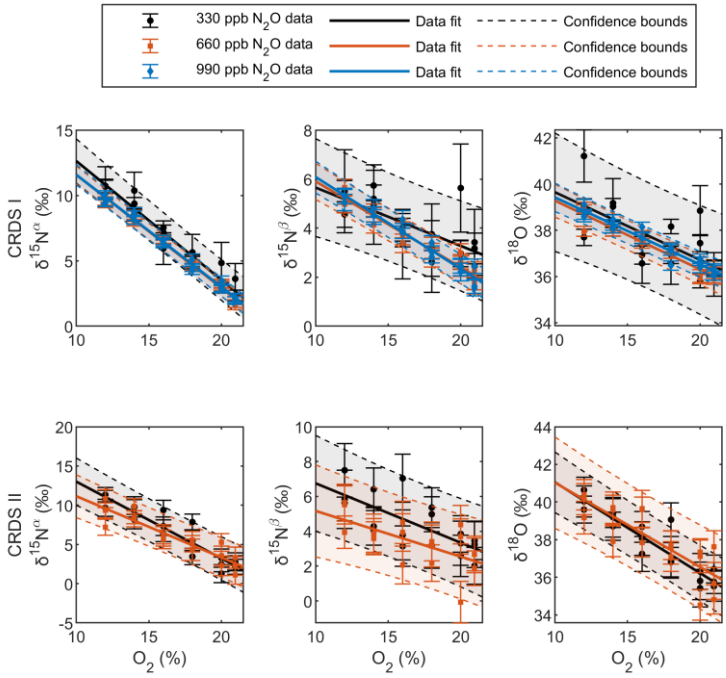


**Figure 8: Apparent changes in $N_2O$ isotopic composition versus $O_2$ concentration change for two CRDS analysers (CRDS I and II). The experimental data points for varying $O_2$ concentration but at a constant $N_2O$ concentration are shown with different colour coding, black (330 ppb), orange (660 ppb) and blue (990 ppb). Each data point corresponds to the mean of three replicate measurements, where each replicate represents an average over 5 minutes. The error bars represent the standard errors, calculated by incorporating the standard deviations from both the sample measurements and the neighbouring calibration gas measurements. The regression line for each $N_2O$ concentration is plotted in black (330 ppb), orange (660 ppb) and blue (990 ppb)6, while shaded areas show the 95% confidence bounds of the corresponding fits.**

Figure 8 shows the effect of $O_2$ concentration changes in the range 12 to 21 % on apparent δ-values. Experiments were repeated thrice for a constant $N_2O$ concentration of 330 ppb, 660 ppb and 990 ppb (CRDS-I) or 330 ppb and 660 ppb (CRDS-II). The experimental data fits well to a linear model, and the regression coefficients, their corresponding uncertainties and the adjusted $R^2$ values are provided in Table 7. The coefficient values are in agreement for the two analyser specimen, for different $N_2O$ concentrations and also with results from Harris et al. (2020). Based on the results, it can be inferred that an instrument-specific correction is applicable for $O_2$ effects on apparent delta values. However, corrections for $\Delta\delta^{15}N^{\beta}$ and $\Delta\delta^{18}O$ at 330 ppb $N_2O$ should be applied with caution, as our experimental data indicate low adjusted $R^2$ values for both CRDS-I and CRDS-II (Fig. 8). A correction term for the $O_2$ matrix gas effect was not included in the MATLAB code, as no relevant oxygen concentration changes are expected for the target application, $N_2O$ emissions from soils.

**Table 7: Experimentally derived correction functions for $O_2$ matrix gas effect of CRDS analysers and simulated results. The correction slope $m_{O2}$ is given in ‰ [% $O_2$]$^{-1}$, the intercept in ‰.**

https://doi.org/10.5194/egusphere-2025-4954
Preprint. Discussion started: 6 November 2025


| Analyser | Date | $\delta^{15}N^{\alpha}$ | | | $\delta^{15}N^{\beta}$ | | | $\delta^{18}O$ | | |
|---|---|---|---|---|---|---|---|---|---|---|
| | | Slope | Intercept | Adj. $R^2$ | Slope | Intercept | Adj. $R^2$ | Slope | Interce pt | Adj. $R^2$ |
| CRDS-I 330 ppb | 05.04.24 (2x), 08.04.24 | -0.91 ± 0.1 | 22.13 | 0.95 | -0.24 ± 0.1 | 8.03 | 0.46 | -0.29 ± 0.1 | 42.58 | 0.43 |
| 660 ppb | 16.04.24 (3x) | -0.86 ± 0.0 | 20.21 | 0.99 | -0.35 ± 0.0 | 9.41 | 0.93 | -0.30 ± 0.0 | 42.26 | 0.92 |
| 990 ppb | 18.04.24 (3x) | -0.86 ± 0.0 | 20.17 | 0.99 | -0.37 ± 0.0 | 9.83 | 0.95 | -0.29 ± 0.0 | 42.33 | 0.93 |
| CRDS-I | Combined coef. | -0.88 ± 0.0 | 20.70 | 0.96 | -0.32 ± 0.0 | 9.09 | 0.75 | -0.29 ± 0.0 | 42.39 | 0.68 |
| CRDS-II 330 ppb | 05.04.24 (2x), 08.04.24 | -0.98 ± 0.1 | 22.8 | 0.87 | -0.34 ± 0.1 | 10.17 | 0.48 | -0.48 ± 0.0 | 45.88 | 0.85 |
| 660 ppb | 16.04.24 (3x) | -0.78 ± 0.1 | 18.96 | 0.84 | -0.26 ± 0.1 | 7.80 | 0.36 | -0.45 ± 0.1 | 45.51 | 0.68 |
| CRDS-II | Combined coef. | -0.88 ± 0.1 | 20.88 | 0.84 | -0.30 ± 0.1 | 8.98 | 0.38 | -0.47 ± 0.0 | 45.69 | 0.76 |
| CRDS-III | (Harris et al. 2020) | -0.89[1)] | | | -0.28[1)] | | | -0.30 | | |

[1)] Correction slopes as given in Fig. S4–4 of Harris et al. (2020) for 330 ppb $N_2O$.

### 3.5 Validation experiments to test combined effects of $N_2O$, $CH_4$ and $CO_2$ concentration changes (Exp. 5)

Experiments involving the simultaneous addition of two interfering gases ($CH_4$ and $CO_2$) at two different $N_2O$ concentrations (330 ppb (Exp. 5a) and 660 ppb (Exp. 5b)) were conducted to assess the practicality of the developed MATLAB code and test whether the established correction functions are additive or require a more complex correction algorithm. Apparent delta values were corrected for $CH_4$ and $CO_2$ spectral interference as well as $N_2O$ non-linearity using the mathematical formalism described in the Appendix (A1) and analyser specific average, i.e. combined, corrections factors given in Table 4– 6. For $CO_2$ interference correction of CRDS-III, correction factors of CRDS-II were applied, which was justified by consistent results for two analyser specimen (CRDS-I and II). Figure 9 and 10 illustrate the combined effects of simultaneously increasing $CH_4$ (0–10 ppm) and $CO_2$ (0–2000 ppm) concentrations on apparent δ-values at two different $N_2O$ concentrations (330 ppb, Fig. 9, 660 ppb, Fig. 10) for the two tested analysers (CRDS-II and III). $CH_4$ and $CO_2$ concentrations were increased stepwise from 0 to 10 ppm (2.5 ppm per step) and 0 to 2000 ppm (500 ppm per step), respectively (see Supplementary Table S11–S12 for further details). Our basic assumption was that spectral interferences by the combined addition of $CH_4$ and $CO_2$ for $\delta^{15}N^{\alpha}$ and $\delta^{18}O$ are predominantly driven by $CH_4$, while interference effects of $CH_4$ and $CO_2$ on $\delta^{15}N^{\beta}$ are more balanced. However, the apparent effects on δ-values resulting from simultaneous $CH_4$ and $CO_2$ addition (Fig. 9, black squares) deviate significantly from the predetermined correction function for $CH_4$-only addition (Fig. 6; Table 5). As a result, the fully corrected delta values (black squares) deviate from actual δ-values for all isotopologues. It is also noteworthy that the correction function for $CH_4/N_2O$ is well-defined with respect to $\delta^{15}N^{\alpha}$ and $\delta^{18}O$ but less substantial for $\delta^{15}N^{\beta}$ (Fig. 6). However, in the validation experiment with simultaneous increases of $CH_4$ and $CO_2$ concentrations, the spectral interference on apparent $\delta^{15}N^{\beta}$ values is substantial (Fig. 9). Another notable observation in this validation experiment is that the observed non-corrected data for $\delta^{15}N^{\alpha}$ agrees

https://doi.org/10.5194/egusphere-2025-4954
Preprint. Discussion started: 6 November 2025


substantially better with $CH_4/N_2O$ correction function derived from spectral simulation than with the one obtained in experiment 2 ($CH_4$ addition without $CO_2$) (not shown). The reasoning for this connection, however, is unclear.

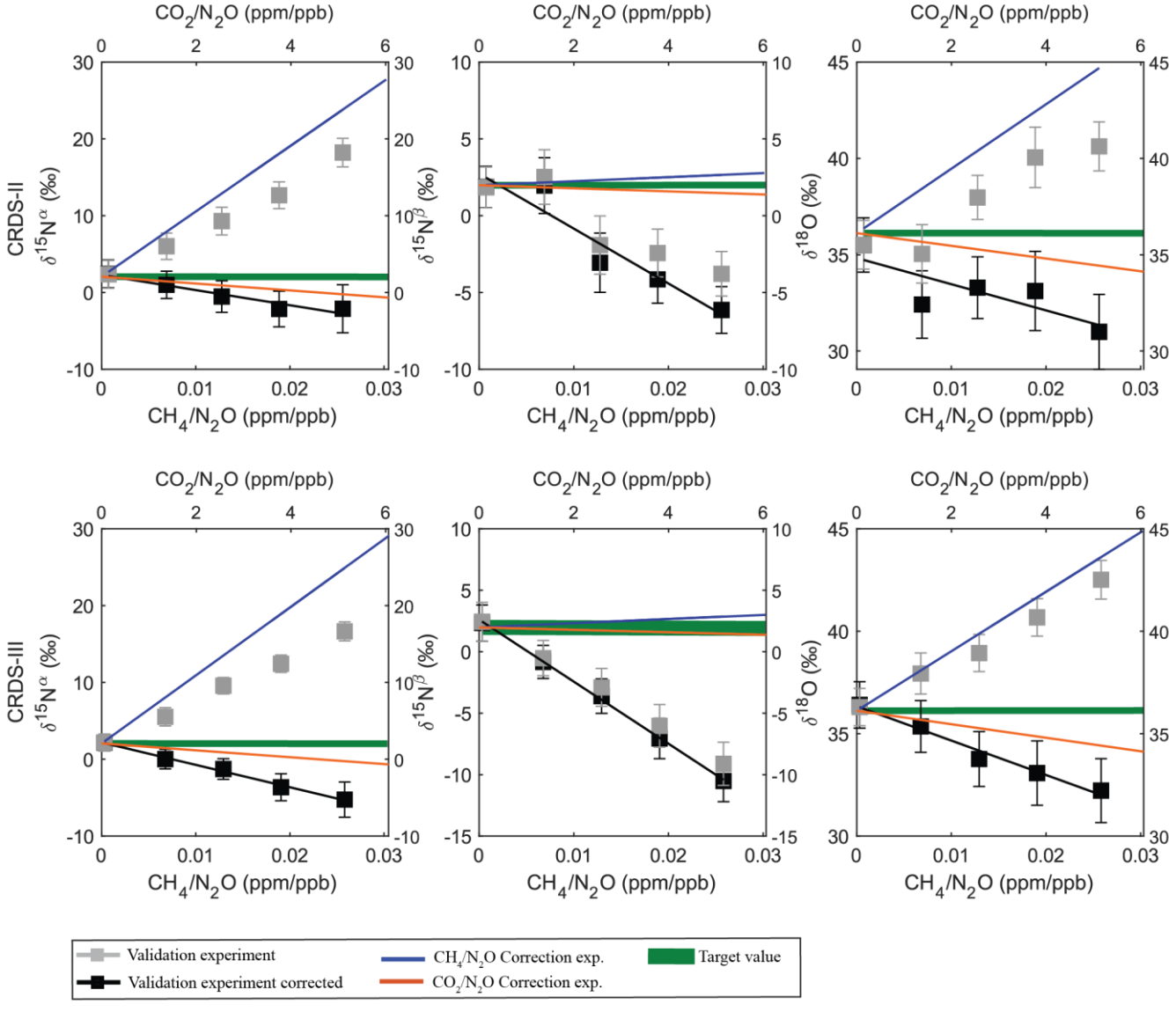


**Figure 9: Interference effects of simultaneous $CH_4$ and $CO_2$ addition on apparent $N_2O$ isotopic composition ($\delta^{15}N^{\alpha}$, $\delta^{15}N^{\beta}$, $\delta^{18}O$) as function of $CH_4/N_2O$ (bottom x-axis) and $CO_2/N_2O$ (top x-axis) concentration ratios. Measurements were conducted at stepwise increasing $CH_4$ and $CO_2$ but constant $N_2O$ (330 ppb) concentration. Grey squares represent experimental data; i.e. apparent data not corrected for $CH_4$ and $CO_2$ effects on δ-values. Solid grey lines indicate linear regression fits to experimental data. Blue solid lines denote, the experimentally determined correction functions for shifts in isotopic compositions with respect to $CH_4/N_2O$ addition, only (Exp 2; Table 5). Likewise, the orange solid lines indicate experimentally determined correction functions for isotopic composition shifts with respect to $CO_2/N_2O$ only (Exp. 3; Table 6). The green area represents $N_2O$ isotopic compositions of the reference gas (Cal $1_{90\ ppm}$; $\delta^{15}N^{\alpha}$ = 2.06 ± 0.05‰, $\delta^{15}N^{\beta}$ = 1.98 ± 0.20‰, $\delta^{18}O$ = 36.12 ± 0.32‰). The black squares represent the δ-**

https://doi.org/10.5194/egusphere-2025-4954
Preprint. Discussion started: 6 November 2025


**values corrected for $CH_4$ and $CO_2$ spectral interferences assuming additive effects of experimentally determined corrections. While for $CH_4$ inference correction analyser specific corrections were applied, for $CO_2$ interference correction, regression factors from CRDS-II were applied for both analysers. Each data point corresponds to the mean of up to three replicate measurements, where each replicate represents an average over 5 minutes. The indicated uncertainty represents the propagated standard error of individual 5-min measurements.**

Validation experiments carried out at 660 ppb $N_2O$ show an even more complex interplay of interference effects (Fig. 10). Our working hypothesis was, that interferences by $N_2O$ non-linearity and $CH_4$ as well as $CO_2$ spectral artifacts, induced by changes in $N_2O$, $CH_4$ and $CO_2$ concentrations of the sample relative to the reference gas, are additive. Experimental results (grey symbols) and δ-values corrected assuming additivity of interferences (black symbols) for CRDS-II display a consistent offset in delta values of up to 15 ‰ for $\delta^{15}N^{\alpha}$ and $\delta^{15}N^{\beta}$ but 20 to 40 ‰ for $\delta^{18}O$. In fact, two datasets were collected on two different measurement dates (20.03.2025 and 20.05.2025). The datasets were corrected using identical $CH_4$ and $CO_2$ regression factors but for the $N_2O$ nonlinearity correction the correction function determined closest to the measurement date were applied (Table 4). Interestingly, measurements at 20.05.2025 (black squared symbols) were corrected with a $N_2O$ non-linearity correction slope, which was determined just a few days before (16.05.2025), and resulted in a better agreement to target values than the second dataset, where $N_2O$ non-linearity (10.04.2025) and validation measurements (20.03.2025) were separated by a longer time interval. For CRDS-III offsets are somewhat smaller for $\delta^{15}N^{\alpha}$ and $\delta^{15}N^{\beta}$ but indicate a decreasing trend with increasing $CH_4$ and $CO_2$ concentrations, similar to measurements at 330 ppb $N_2O$. Corrected results for $\delta^{18}O$ analysed by CRDS-III show an approximately 25 ‰ offset. We speculate, that persistent offsets between corrected delta values to the target are linked to the observed changes in the $N_2O$ non-linearity correction function over time (Fig. 5; Table 4)

https://doi.org/10.5194/egusphere-2025-4954
Preprint. Discussion started: 6 November 2025


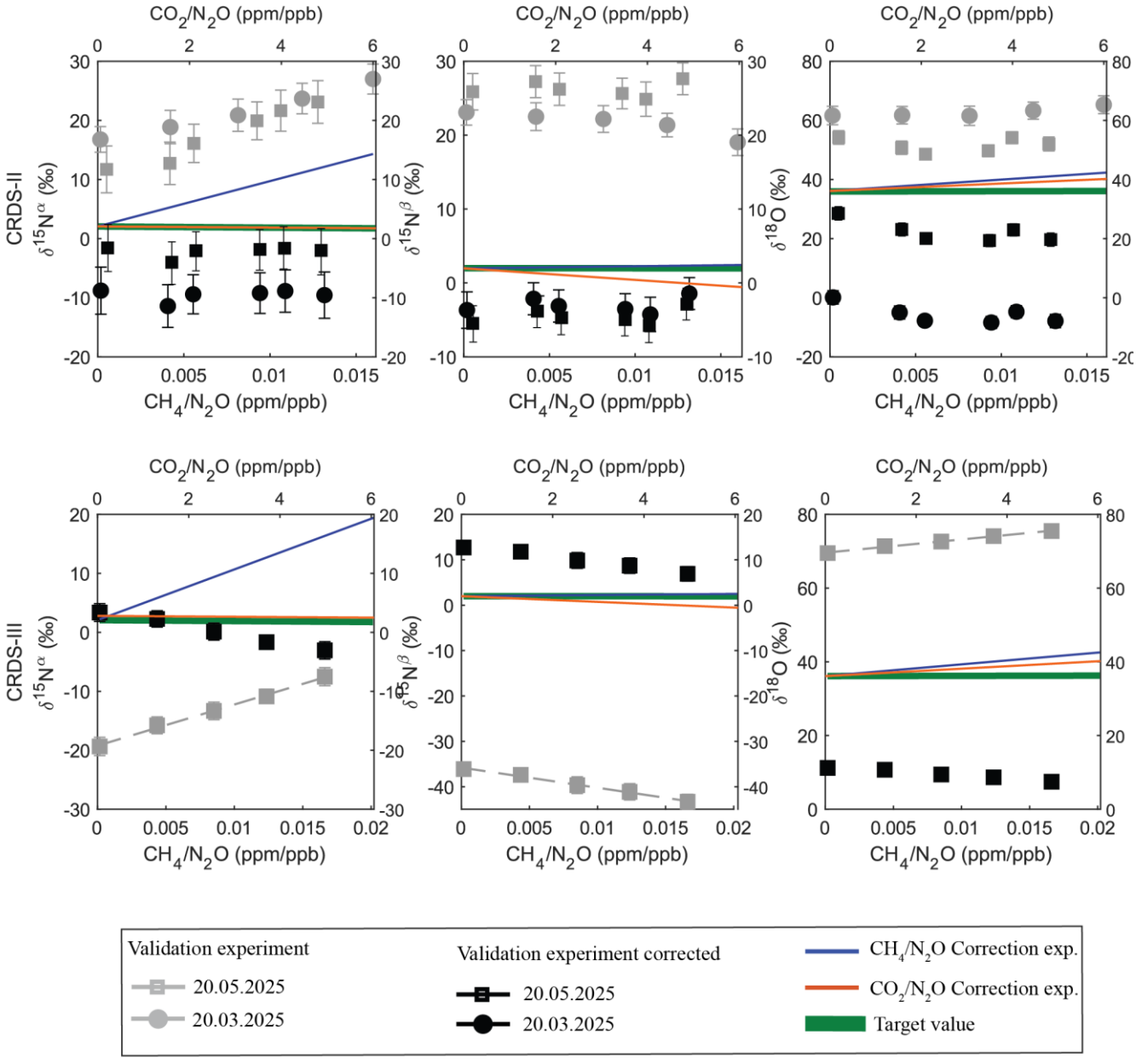


**Figure 10: Interference effects of simultaneous changes in $N_2O$, $CH_4$ and $CO_2$, relative to reference gas composition on the apparent $N_2O$ isotopic composition ($\delta^{15}N^{\alpha}$, $\delta^{15}N^{\beta}$, $\delta^{18}O$) as functions of $CH_4/N_2O$ (bottom x-axis) and $CO_2/N_2O$ (top x-axis) concentration ratios at constant $N_2O$ (660 ppb). Grey squares represent experimental, i.e. apparent data not corrected for $CH_4$ and $CO_2$ effects on δ-values. Solid grey lines indicate linear regression fits to experimental data. The blue solid line denotes the experimentally determined correction function for shifts in isotopic compositions with respect to $CH_4/N_2O$ mixtures without simultaneous addition of $CO_2$ (Exp 2; Table 6). Likewise, the orange solid line indicates the experimentally determined correction function for isotopic composition shift with respect to $CO_2/N_2O$ mixtures without concurrent addition of $CH_4$ (Exp. 3; Table 5). The green area represents $N_2O$ isotopic compositions of the reference gas (Cal $1_{90\ ppm}$; $\delta^{15}N^{\alpha} = 2.06 \pm 0.05$‰, $\delta^{15}N^{\beta} = 1.98 \pm 0.20$‰, $\delta^{18}O = 36.12 \pm 0.32$‰). The black squares represent δ-values corrected for differences in $N_2O$, $CH_4$ and $CO_2$ concentrations, relative to reference gases, assuming additivity of interferences. For $N_2O$ and $CH_4$ interference correction analyser specific corrections were applied, for $CO_2$ regression factors**

https://doi.org/10.5194/egusphere-2025-4954
Preprint. Discussion started: 6 November 2025


**determined for CRDS-II were used for both analysers. Each data point corresponds to the mean of up to three replicate measurements, where each replicate represents an average over 5 minutes. The indicated uncertainty represents the propagated standard error of individual 5-min measurements.**

## 4. Discussion

We implemented and parametrised the mathematical framework for the correction and calibration of $N_2O$ isotopic data in a stand-alone MATLAB code. More specifically, output data of the CRDS analyser model G5131-*i* (Picarro Inc., USA) was used and corrections relevant for $N_2O$ emissions from soils applied. The tested CRDS analyser model G5131-*i* has the potential for real-time analysis of the $N_2O$ site-specific isotopic composition ($\delta^{15}N^{\alpha}$, $\delta^{15}N^{\beta}$) as well as $\delta^{18}O$ in ambient $N_2O$ at high precision (< 1 ‰). To provide accurate data, relevant differences in gas composition between the sample and the applied isotope reference gases have to be assessed and, if necessary, corrected. It is best practice to adapt the gas composition of isotope reference gases to match the sample; however, most applications involve inevitable changes in gas concentrations, which must be either eliminated or considered. For the target application of this study, $N_2O$ emissions from soil, changes in $N_2O$, $CH_4$, $CO_2$ and $H_2O$ concentrations are expected to occur. The implemented correction terms for $N_2O$ non-linearity, spectral interferences by $CH_4$, $CO_2$ or $H_2O$, gas matrix and drift effects and calibration to international isotope ratio scales are more widely applicable and in line with guidelines developed for other isotope systems ($CO_2$ and $CH_4$) and analyser models (Braden-Behrens et al., 2023; Sperlich, 2024). We tested the applicability of correction terms beyond a single analyser specimen and over time, comparing interference effects across three individual instruments, with published data for the G5131-*i* analyser model (Harris et al., 2020) and spectral simulations. Finally, the additivity of correction terms for interference effects was tested in a validation study for simultaneous changes in $CH_4$, $CO_2$, and $N_2O$ concentrations. Different aspects of our study are discussed in more detail below.

### 4.1 Limitations and operational requirements for G5131-*i*

#### 4.1.1 Non-additive behaviour of correction terms

Results of the first validation experiments (Fig. 9), in which $CH_4$ and $CO_2$ concentrations were changed simultaneously in sample gases with respect to isotopic reference gases, indicate that the spectral interference effects of $CH_4$ and $CO_2$ on apparent delta values are non-additive, which contradicts our prior assumption. Spectral interferences by changes in $CH_4$ concentration alone were found to be independent of the analyser specimen and constant over time, and therefore can be effectively corrected. Interestingly, experimentally determined $CO_2$ interferences were smaller than anticipated from spectral simulations, indicating that the raw data were post-corrected by the analyser software. We therefore speculate whether the presence of $CH_4$ may mislead the $CO_2$ post-correction algorithm implemented in the analyser software, resulting in the observed offsets. Alternatively, the presence of $CO_2$ may reduce spectral interferences from $CH_4$, thereby increasing absorption towards a non-linear regime in specific wavelength regions. The tested scenarios with up to 2'000 ppm $CO_2$ and 10 ppm $CH_4$ changes might

https://doi.org/10.5194/egusphere-2025-4954
Preprint. Discussion started: 6 November 2025


be realistic for some applications in the agricultural sector (e.g. dairy housing; Schrade et al., 2023) but are too strict for $N_2O$ studies in upland soils, where $CH_4$ concentrations changes are substantially smaller (e.g. 50–300 ppb $CH_4$). If two or more relevant spectral interferents are present, we suggest avoiding additive spectral-interference correction, because it can lead to inaccurate results. Instead, interferants should be removed using adsorbents or catalysts, e.g. $CO_2$ by alkaline sorbents. The spectral interference of the residual interferant can then be corrected accurately. Alternatively, one might consider developing and implementing more complex two- or multi-dimensional interference correction schemes, which, however, is beyond the focus of our study.

#### 4.1.2 Temporally variable $N_2O$ non-linearity correction

Results of the second validation experiment (Fig. 10), conducted at 660 ppb $N_2O$, exhibit an even more complex interplay of $N_2O$ non-linearity and $CO_2$ as well as $CH_4$ spectral interference. In fact, corrected measurement data for samples without $CH_4$ and $CO_2$ addition but only change in $N_2O$ concentration (660 ppb as compared to 330 ppb for the reference gas), indicate in some cases agreement with the target composition within a few per mille but often more significant offsets. This discrepancy is most likely due to a drift in the $N_2O$ non-linearity correction over time. Similarly, drift effects in $N_2O$ non-linearity are indicated by replicate measurements over time for the same analyser specimen (Table 4). In addition, replicate measurements show better agreement of corrected data with target composition when correction parameters are determined shortly before or after. Challenges with appropriate $N_2O$ non-linearity correction are largest for $\delta^{18}O$, less severe for $\delta^{15}N^{\alpha}$ and $\delta^{15}N^{\beta}$. Corrected results for samples with enhanced $N_2O$ concentration as well as $CH_4$ and $CO_2$ concentrations show a constant offset to target values, independent of $CH_4$ and $CO_2$ concentrations, for one analyser, while the second instrument shows an additional effect on non-additive $CH_4$ and $CO_2$ interference corrections. To ensure accurate $N_2O$ isotopologue analysis using a G5131-*i* analyser, we recommend one of two alternative approaches. Either diluting the sample gas to ambient $N_2O$ concentrations with full synthetic air (matrix c), thereby avoiding the need for a $N_2O$ non-linearity correction, or analysing the $N_2O$ non-linearity directly before/after each sample measurement sequence to ensure the correction function reflects the current instrumental conditions.

### 4.2 Recommendations and Best Practices for field measurements

In accordance with the results obtained from our study, we confirm the basic step-by-step workflow presented by Harris et al. (2020) for the G5131-*i* analyser but would like to refine several points, most importantly:

- The spectral interference on $N_2O$ delta values measured by the CRDS analyser was found to be linearly dependent on the concentration of the spectral interferant (e.g. $CH_4$ or $CO_2$) and the inverse concentration of the target gas ($N_2O$).

https://doi.org/10.5194/egusphere-2025-4954
Preprint. Discussion started: 6 November 2025


- For the tested analyser model the $CH_4$ spectral interference on delta values was found to be of no significant difference for different analyser specimen, which would warrant the use of model specific correction terms. For post correction of delta values, parallel measurements with a specific $CH_4$ concentration analyser are required.
- Spectral interferences of different substances (e.g. $CH_4$ and $CO_2$) on $N_2O$ δ-values were found to be non-additive, suggesting either removal of one interferant (e.g. $CO_2$) and correction of the second, or development of a more sophisticated correction model.
- The gas matrix effect of changes in the oxygen concentration on δ values was found to be independent of the $N_2O$ target gas concentration, which simplifies corrections. Additivity of gas matrix effects and spectral interferences were not tested.
- $N_2O$ non-linearity correction of delta values of the G5131-*i* analyser was found to be highly variable with time; we therefore suggest determining dependencies with a sufficiently high temporal resolution or diluting sample gases to ambient $N_2O$ concentrations, covered by reference gases, using an appropriate dilution gas.

The established mathematical framework was implemented in a MATLAB code, parametrised and is applicable for other isotope systems or detection schemes but should be validated with care for the specific application before use.

### 4.3 Outlook and Future Work

A key outcome of this work is the development of a streamlined and easy-to-use post-processing protocol for isotopic data obtained on laser spectrometers in general and exemplified here by $N_2O$ isotope data obtained with a G5131-*i* analyser from Picarro Inc. (USA). By combining analyser-specific $N_2O$ non-linearity corrections with universally applicable corrections (e.g., $CH_4$) and by incorporating a GUM-compliant uncertainty analysis, we provide a stand-alone and user-friendly MATLAB post-processing routine for obtaining calibrated $N_2O$ isotopic data. We suggest a future community effort to implement our workflow and accompanying MATLAB algorithm to ensure that $N_2O$ isotope datasets generated at different laboratories are directly comparable and not affected by programming flaws. Furthermore, standardisation accelerates progress and therefore, this protocol can be used as a baseline while simultaneously updating the shared code as new analyser models, wavelength regions or calibration schemes emerge.

Future challenges lie in addressing the apparent non-additive interferences, such as the one observed between $CH_4$ and $CO_2$, where the combined effect of two interference gases on the δ-values cannot be predicted by simply summing up the individual correction terms. A key next step might be to characterise this behaviour systematically and potentially embed a dedicated $CH_4$-$CO_2$ interaction coefficient into the post-processing routine. Extending experimental investigations of non-additive effects to other interference gases, $CH_4$ and $O_2$, will further broaden the applicability of this protocol.

Finally, for long-term field deployment of analysers, the robustness of the post-processing protocol has to be tested outside a controlled laboratory setting. Although field operation inevitably introduces additional variability to the measurements, a thorough understanding of critical interferences and a standardised data-reduction workflow should make high-quality $N_2O$

https://doi.org/10.5194/egusphere-2025-4954
Preprint. Discussion started: 6 November 2025


isotope measurements manageable under real-world conditions. This will provide valuable insights into the biogeochemical cycling of this potent greenhouse gas.

## Data availability

All raw data can be provided upon request to the corresponding authors.

## Author Contributions

Julius C. Havsteen drafted the manuscript, performed data acquisition, and contributed to the development of the framework and logic underlying the data correction strategy. Mehr Fatima produced most of the figures, conducted experimental work and data analysis, and contributed to the improvement of the manuscript. Simone Brunamonti developed the MATLAB code and derived the mathematical framework for the reduction algorithm. Andrea Pogány simulated the data and provided expertise on CRDS instruments. Thomas Hausmaninger supported data visualisation and statistical analysis. Benjamin Wolf and Reinhard Well each provided a Picarro G5131-*i* instrument and assisted with manuscript proofreading. Joachim Mohn made significant contributions to editing the manuscript, deriving the mathematical framework, and refining the overall structure and flow.

## Competing interests

The authors declare no competing interests.

## Acknowledgements

We acknowledge Kerstin Zeyer, Hannes Keck, Nicholas Gianotti and Giulio Milani for their help and support in establishing the analytical setup and the MATLAB code, as well as collecting the analyser data. Christoph Zellweger (WCC Empa) was instrumental in assigning greenhouse gas concentration values to our calibration gases on NOAA WMO GAW scales.

## Financial Support

This work is part of the project 21GRD10 quantiAGREMI, which has received funding from the European Partnership on Metrology, co-financed from the European Union's Horizon Europe Research and Innovation Programme and by the Participating States. In addition, the project was financed by the European Union's Horizon Europe Research and Innovation

https://doi.org/10.5194/egusphere-2025-4954
Preprint. Discussion started: 6 November 2025


programme under HORIZON-CL5-2022-D1-02 Grant Agreement No 101081430 – PARIS. The Empa contribution has received funding from the Swiss State Secretariat for Education, Research and Innovation (SERI).

# Appendix

## A1. Mathematical formulation of the data processing algorithm

Here we report the mathematical equations used for all corrections implemented in the data analysis algorithm. The main parameters are the $N_2O$ concentration ([$N_2O$]) and the $\delta$-values of the different isotopologues ($\delta^{15}N^{\alpha}$, $\delta^{15}N^{\beta}$, $\delta^{18}O$) obtained from the G5131-*i* analyser, and the $CH_4$, CO and $CO_2$ concentrations ([$CH_4$], [CO], [$CO_2$]) from the G2401 analyser. Note that, for brevity, the corrections on apparent delta-values are expressed below for a generic isotopologue ($\delta$), while all equations are applied to all three measured isotopologues ($\delta^{15}N^{\alpha}$, $\delta^{15}N^{\beta}$, $\delta^{18}O$).

### A1.1. Pre-processing

First, the measurement intervals (*plateau*) are identified and labelled by gas type as described in Section 2.4.1, and all data are averaged to a user-defined integration time (e.g., 15 s). All data points outside the *plateau* intervals are discarded, and the mean and standard deviations are calculated for each interval and gas type according to Eq. A1–A4. Superscripts *Mean* and $Int_k$ indicate quantities calculated over the entire experimental sequence and an individual measurement interval ($k$), respectively. Subscript *Sample* indicates a generic gas sample, which can be either a reference gas (*Cal 1*, *Cal 2*) or a generic sample (e.g., $Sample_1$, $Sample_2$, etc.).

$$\delta_{Sample}^{Mean} = \frac{1}{N}\sum_{i=1}^{N}\delta_{Sample,i} \quad where\ i = 1, \dots, N\ are\ all\ data\ points\ that\ belong\ to\ Sample\ gas \tag{A1}$$

$$\sigma_{Sample}^{Mean} = \sqrt{\frac{1}{N-1}\sum_{i=1}^{N}(\delta_{Sample,i} - \delta_{Sample}^{Mean})^2} \tag{A2}$$

$$\delta_{Sample}^{Int_k} = \frac{1}{K}\sum_{j=1}^{K}\delta_{Sample,j} \quad where\ j = 1, \dots, K\ are\ all\ data\ points\ that\ belong\ to\ Interval\ k \tag{A3}$$

$$\sigma_{Sample}^{Int} = \sqrt{\frac{1}{K-1}\sum_{j=1}^{K}(\delta_{Sample,j} - \delta_{Sample}^{Int_k})^2} \tag{A4}$$

https://doi.org/10.5194/egusphere-2025-4954
Preprint. Discussion started: 6 November 2025


### A1.2. Instrumental parameters

The raw data are checked for potential correlations with G5131-*i* instrumental parameters, particularly cell pressure ($p_{Cell}$), cell temperature ($T_{Cell}$), chiller temperature ($T_{Chiller}$), and P9 (i.e., back-mirror) temperature ($T_{P9}$), by means of a "correlation matrix" plot of [$N_2O$] and all $\delta$-values against all instrumental parameters (including $R^2$ correlation coefficients) that can be generated by the code, allowing the user to easily identify anomalous correlation. In case a significant correlation is observed, [$N_2O$] and the $\delta$-values can be corrected applying Eq. A5–A6, where $Y$ represents one of the instrumental parameters listed above ($p_{Cell}$, $T_{Cell}$, $T_{Chiller}$, $T_{P9}$). The slope $m$ of the correction function is determined by a linear fit between the apparent $N_2O$ concentration (or $\delta$-value) and the considered controlling parameter, recorded during anchor or calibration gas 1 (*Cal 1*) measurements.

$$[N_2O]_{Sample} = [N_2O]^{Raw}_{Sample} - m_1\left(Y_{Sample} - Y^{Mean}_{Cal_1}\right) \quad \text{(A5)}$$

$$\delta_{Sample} = \delta^{Raw}_{Sample} - m_2\left(Y_{Sample} - Y^{Mean}_{Cal_1}\right) \quad \text{(A6)}$$

### A1.3. Correction of concentration data

The concentration data are corrected (superscript *Corr*) and calibrated (superscript *Calib*) by a drift correction (Eq. A7–A8) and a calibration correction (A9–A10), where [$X$] represents either [$N_2O$], [$CH_4$], [CO] or [$CO_2$]. For each sample interval, the "offset" due to drift is calculated as the difference between the linear interpolation of the two nearest (bracketing) *Cal 1* intervals (*Int(+)*, *Int(−)*) and its mean value over all *Cal 1* intervals. Consequently, all *Cal 1* measurements are corrected to their mean value. The calibration can be either a one- or two-point calibration correction, depending on the number of available reference gases ($Cal_2$: calibration gas 2). Superscript *True* indicates the given "true" value of the reference gases.

$$[X]^{Corr}_{Sample} = [X]^{Raw}_{Sample} - \Delta[X]_{Drift} \quad \text{(A7)}$$

$$\Delta[X]_{Drift} = \frac{[X]^{Int(-),Raw}_{Cal_1} \cdot \left(t_{Sample} - t^{Int(-)}_{Cal_1}\right) + [X]^{Int(+),Raw}_{Cal_1} \cdot \left(t^{Int(+)}_{Cal_1} - t_{Sample}\right)}{t^{Int(+)}_{Cal_1} - t^{Int(-)}_{Cal_1}} - [X]^{Mean,Raw}_{Cal_1} \quad \text{(A8)}$$

$$[X]^{Corr,Calib}_{Sample} = \begin{cases} [X]^{Corr}_{Sample} - \left([X]^{Mean,Corr}_{Cal_1} - [X]^{True}_{Cal_1}\right) & (1-point\ calibration) \\ y_X \cdot \left([X]^{Corr}_{Sample} - [X]^{Mean,Corr}_{Cal_1}\right) + [X]^{True}_{Cal_1} & (2-point\ calibration) \end{cases} \quad \text{(A9)}$$

$$y_X = \frac{[X]^{True}_{Cal_1} - [X]^{True}_{Cal_2}}{[X]^{Mean,Corr}_{Cal_1} - [X]^{Mean,Corr}_{Cal_2}} \quad \text{(A10)}$$

### A1.4. Correction of $\delta$-values

The raw $\delta$-values retrieved by the spectrometer can be corrected and calibrated by the sequential application of the $N_2O$ concentration (Eq. 12), $CH_4$ and $CO_2$ spectral interference corrections (Eq. 13–14), drift correction (Eq. 15), and calibration correction (Eq. 16–17). The slopes of the $N_2O$ concentration and spectral interference corrections ($m_{N_2O}, m_{CH_4}, m_{CO_2}$) are instrument-specific and must be defined by the user for each of the measured isotopologues ($^{15}N^{\alpha}$, $^{15}N^{\beta}$, $^{18}O$). Again, the calibration correction can be either a one- or two-point calibration, depending on the number of available reference gases

https://doi.org/10.5194/egusphere-2025-4954
Preprint. Discussion started: 6 November 2025


$$\delta_{Sample}^{Corr} = \delta_{Sample}^{Raw} - \Delta\delta_{N2O} - \Delta\delta_{CH4} - \Delta\delta_{CO2} - \Delta\delta_{Drift} \quad \text{(A11)}$$

$$\Delta\delta_{N_2O} = m_{N_2O}\left(\frac{1}{[N_2O]_{Sample}^{Corr,Calib}} - \frac{1}{[N_2O]_{Cal_1}^{True}}\right) \quad \text{(A12)}$$

$$\Delta\delta_{CH_4} = m_{CH_4}\left(\frac{[CH_4]_{Sample}^{Corr,Calib}}{[N_2O]_{Sample}^{Corr,Calib}} - \frac{[CH_4]_{Cal_1}^{True}}{[N_2O]_{Cal_1}^{True}}\right) \quad \text{(A13)}$$

$$\Delta\delta_{CO_2} = m_{CO_2}\left(\frac{[CO_2]_{Sample}^{Corr,Calib}}{[N_2O]_{Sample}^{Corr,Calib}} - \frac{[CO_2]_{Cal_1}^{True}}{[N_2O]_{Cal_1}^{True}}\right) \quad \text{(A14)}$$

$$\Delta\delta_{Drift} = \frac{\delta_{Cal_1}^{Int(-),Raw} \cdot \left(t_{Sample} - t_{Cal_1}^{Int(-)}\right) + \delta_{Cal_1}^{Int(+),Raw} \cdot \left(t_{Cal_1}^{Int(+)} - t_{Sample}\right)}{t_{Cal_1}^{Int(+)} - t_{Cal_1}^{Int(-)}} - \delta_{Cal_1}^{Mean,Raw} \quad \text{(A15)}$$

$$\delta_{Sample}^{Corr,Calib} = \begin{cases} \delta_{Sample}^{Corr} - \left(\delta_{Cal_1}^{Mean,Corr} - \delta_{Cal_1}^{True}\right) & (1-\text{point calibration}) \\ y \cdot \left(\delta_{Sample}^{Corr} - \delta_{Cal_1}^{Mean,Corr}\right) + \delta_{Cal_1}^{True} & (2-\text{point calibration}) \end{cases} \quad \text{(A16)}$$

$$y = \frac{\delta_{Cal_1}^{True} - \delta_{Cal_2}^{True}}{\delta_{Cal_1}^{Mean,Corr} - \delta_{Cal_2}^{Mean,Corr}} \quad \text{(A17)}$$

### A1.5. Uncertainty propagation

Finally, the code offers the possibility to calculate the propagated uncertainty ($u$) on the final $\delta$-values associated with all the applied corrections and calibration, using the error propagation law (Eq. A18–A19). Five error sources ($U$) are considered and must be defined by the user for each isotopologue, including uncertainties in the slopes used for the $N_2O$ concentration correction and spectral interference corrections ($m_{N_2O}, m_{CH_4}, m_{CO_2}$), uncertainties in the "true" $\delta$-values attributed to reference gases ($\delta_{Cal_1}^{True}, \delta_{Cal_2}^{True}$), plus an additional term representing "poorly understood" effects ($u_{Other}$), which can be approximated by repeatability for target gas measurements.

$$U = \left(m_{N_2O}, m_{CH_4}, m_{CO_2}, \delta_{Cal_1}^{True}, \delta_{Cal_2}^{True}\right) \quad \text{(A18)}$$

$$u_{Sample}^{Corr,Calib} = \sqrt{\sum_{i=1}^{5}\left(\frac{\partial\delta_{Sample}^{Corr,Calib}}{\partial U_i}\Delta U_i\right)^2 + u_{Other}^2} \quad \text{(A19)}$$

Solving the partial derivatives of Eq. A19 for a 2-point calibration correction (see Eq. A16) yields:

$$\frac{\partial\delta_{Sample}^{Corr,Calib}}{\partial m_{N_2O}}\Delta m_{N_2O} = y\left(\frac{1}{[N_2O]_{Sample}^{Corr,Calib}} - \frac{1}{[N_2O]_{Cal_1}^{True}}\right)\Delta m_{N_2O} \quad \text{(A20)}$$

$$\frac{\partial\delta_{Sample}^{Corr,Calib}}{\partial m_{CH_4}}\Delta m_{CH_4} = y\left(\frac{[CH_4]_{Sample}^{Corr,Calib}}{[N_2O]_{Sample}^{Corr,Calib}} - \frac{[CH_4]_{Cal_1}^{True}}{[N_2O]_{Cal_1}^{True}}\right)\Delta m_{CH_4} \quad \text{(A21)}$$

https://doi.org/10.5194/egusphere-2025-4954
Preprint. Discussion started: 6 November 2025


$$\frac{\partial \delta_{Sample}^{Corr,Calib}}{\partial m_{CO_2}} \Delta m_{CO_2} = y \left( \frac{[CO_2]_{Sample}^{Corr,Calib}}{[N_2O]_{Sample}^{Corr,Calib}} - \frac{[CO_2]_{Cal_1}^{True}}{[N_2O]_{Cal_1}^{True}} \right) \Delta m_{CO2} \quad \text{(A22)}$$

$$\frac{\partial \delta_{Sample}^{Corr,Calib}}{\partial \delta_{Cal_1}^{True}} \Delta \delta_{Cal1}^{True} = \left( \frac{\delta_{Sample}^{Corr} - \delta_{Cal_2}^{Mean,Corr}}{\delta_{Cal_1}^{Mean,Corr} - \delta_{Cal_2}^{Mean,Corr}} \right) \Delta \delta_{Cal1} \quad \text{(A23)}$$

$$\frac{\partial \delta_{Sample}^{Corr,Calib}}{\partial \delta_{Cal_2}^{True}} \Delta \delta_{Cal_2}^{True} = \left( \frac{\delta_{Cal_1}^{Mean,Corr} - \delta_{Sample}^{Corr}}{\delta_{Cal_1}^{Mean,Corr} - \delta_{Cal_2}^{Mean,Corr}} \right) \Delta \delta_{Cal_2} \quad \text{(A24)}$$

Solving the partial derivatives of Eq. A19 for a 1-point calibration correction (i.e., $\Delta \delta_{Cal_2}^{True} = 0$) yields:

$$\frac{\partial \delta_{Sample}^{Corr,Calib}}{\partial m_{N_2O}} \Delta m_{N_2O} = \left( \frac{1}{[N_2O]_{Sample}^{Corr,Calib}} - \frac{1}{[N_2O]_{Cal_1}^{True}} \right) \Delta m_{N_2O} \quad \text{(A25)}$$

$$\frac{\partial \delta_{Sample}^{Corr,Calib}}{\partial m_{CH_4}} \Delta m_{CH_4} = \left( \frac{[CH_4]_{Sample}^{Corr,Calib}}{[N_2O]_{Sample}^{Corr,Calib}} - \frac{[CH_4]_{Cal_1}^{True}}{[N_2O]_{Cal_1}^{True}} \right) \Delta m_{CH_4} \quad \text{(A26)}$$

$$\frac{\partial \delta_{Sample}^{Corr,Calib}}{\partial m_{CO_2}} \Delta m_{CO_2} = \left( \frac{[CO_2]_{Sample}^{Corr,Calib}}{[N_2O]_{Sample}^{Corr,Calib}} - \frac{[CO_2]_{Cal_1}^{True}}{[N_2O]_{Cal_1}^{True}} \right) \Delta m_{CO2} \quad \text{(A27)}$$

$$\frac{\partial \delta_{Sample}^{Corr,Calib}}{\partial \delta_{Cal_1}^{True}} \Delta \delta_{Cal_1}^{True} = \Delta \delta_{Cal_1} \quad \text{(A28)}$$

https://doi.org/10.5194/egusphere-2025-4954
Preprint. Discussion started: 6 November 2025


## References

Barnes, J. and Allan, D.: Statistics of atomic frequency standards, Proc. IEEE, 54, 221 - 230, https://doi.org/10.1109/PROC.1966.4634, 1966.

Braden-Behrens, J., Emad, A., Ebert, V., Durbiano, F., Li, G., Moossen, H., Nwaboh, J., Pavarelli, S., Rolle, F., Sega, M., and Steur, P. M.: Good practice guide for specification and application of OIRS for atmospheric measurements, including sample handling protocol, optimised analytical procedures, traceability to the international standards and target uncertainties (0.05 ‰ for δ13C-CO2 and δ18O-CO2), Physikalisch-Technische Bundesanstalt, Braunschweig, Germany, 2023.

Denk, T. R., Kraus, D., Kiese, R., Butterbach-Bahl, K., and Wolf, B.: Constraining N cycling in the ecosystem model LandscapeDNDC with the stable isotope model SIMONE, Ecology, 100, e02675, https://doi.org/10.1002/ecy.2675, 2019.

Forster, P., Ramaswamy, V., Artaxo, P., Berntsen, T., Betts, R., Fahey, D. W., Haywood, J., Lean, J., Lowe, D. C., Myhre, G., Nganga, J., Prinn, R., Raga, G., Schulz, M., and Van Dorland, R.: Changes in atmospheric constituents and in radiative forcing, in: Climate Change 2007: The Physical Science Basis, edited by: Solomon, S., Qin, D., Manning, M., Chen, Z., Marquis, M., Averyt, K. B., Tignor, M., and Miller, H. L., Cambridge University Press, Cambridge, United Kingdom; New York, NY, USA, 129–234, 2007.

Gordon, I. E., Rothman, L. S., Hargreaves, R. J., Hashemi, R., Karlovets, E. V., Skinner, F. M., Conway, E. K., Hill, C., Kochanov, R. V., and Tan, Y.: The HITRAN2020 molecular spectroscopic database, J. Quant. Spectrosc. Radiat. Transf., 277, 107949, https://doi.org/10.1016/j.jqsrt.2021.107949, 2022.

Gruber, W., Magyar, P. M., Mitrovic, I., Zeyer, K., Vogel, M., von Känel, L., Biolley, L., Werner, R. A., Morgenroth, E., and Lehmann, M. F.: Tracing N2O formation in full-scale wastewater treatment with natural abundance isotopes indicates control by organic substrate and process settings, Water Res. X, 15, 100130, https://doi.org/10.1016/j.wroa.2022.100130, 2022.

Harris, S. J., Liisberg, J., Xia, L., Wei, J., Zeyer, K., Yu, L., Barthel, M., Wolf, B., Kelly, B. F., and Cendón, D. I.: N2O isotopocule measurements using laser spectroscopy: analyzer characterization and intercomparison, Atmos. Meas. Tech., 13, 2797-2831, https://doi.org/10.5194/amt-13-2797-2020, 2020.

JCGM: Evaluation of measurement data—Guide to the expression of uncertainty in measurement Joint Committee for Guides in Metrology (JCGM), Sèvres, FranceJCGM 100:2008, https://doi.org/10.59161/JCGM100-2008E, 2008.

Lan, X., Thonning, K. W., and Dlugokencky, E. J.: Trends in globally-averaged CH4, N2O, and SF6 determined from NOAA Global Monitoring Laboratory measurements. Version 2024-11, https://doi.org/10.15138/P8XG-AA10, 2024.

Mohn, J., Biasi, C., Bodé, S., Boeckx, P., Brewer, P. J., Eggleston, S., Geilmann, H., Guillevic, M., Kaiser, J., and Kantnerová, K.: Isotopically characterised N2O reference materials for use as community standards, Rapid Commun. Mass Spectrom., 36, e9296, https://doi.org/10.1002/rcm.9296, 2022.

Ostrom, N. E., Gandhi, H., Coplen, T. B., Toyoda, S., Böhlke, J. K., Brand, W. A., Casciotti, K. L., Dyckmans, J., Giesemann, A., and Mohn, J.: Preliminary assessment of stable nitrogen and oxygen isotopic composition of USGS51 and USGS52 nitrous oxide reference gases and perspectives on calibration needs, Rapid Commun. Mass Spectrom., 32, 1207-1214, https://doi.org/10.1002/rcm.8157, 2018.

Pogány, A., Lüttschwager, N. O. B., Banik, G. D., Persijn, S., de Boed, E. J. J., Sutour, C., Macé, T., Nwaboh, J. A., Werhahn, O., and Ebert, V.: Towards an optical gas standard for ammonia measurements in air at ambient levels, J. Quant. Spectrosc. Radiat. Transf., 347, 109643, https://doi.org/10.1016/j.jqsrt.2025.109643, 2025.

Schrade, S., Zeyer, K., Mohn, J., and Zähner, M.: Effect of diets with different crude protein levels on ammonia and greenhouse gas emissions from a naturally ventilated dairy housing, Science of The Total Environment, 896, 165027, https://doi.org/10.1016/j.scitotenv.2023.165027, 2023.

Sperlich, P., Camin, F., Deufrains, K., Eglund Michel, S., Hoheisel, A., Mohn, J., Schmidt, M., Tarasova, O. : Measurement of the Stable Carbon Isotope Ratio in Atmospheric CH4 Using Laser Spectroscopy for CH4 Source Characterization, International Atomic Energy Agency (IAEA), Vienna, IAEA-TECDOC-2066, https://doi.org/10.61092/iaea.logm-wiux, 2024.

https://doi.org/10.5194/egusphere-2025-4954
Preprint. Discussion started: 6 November 2025


Toyoda, S. and Yoshida, N.: Determination of nitrogen isotopomers of nitrous oxide on a modified isotope ratio mass spectrometer, Anal. Chem., 71, 4711-4718, https://doi.org/10.1021/ac9904563, 1999.
Toyoda, S., Yoshida, N., and Koba, K.: Isotopocule analysis of biologically produced nitrous oxide in various environments, Mass Spectrom. Rev., 36, 135-160, https://doi.org/10.1002/mas.21459, 2017.
Wanlu, W., Lingling, Z., Di, Z., Zhe, S., and Biao, J.: Spectroscopic techniques to analyze stable carbon isotopic compositions of carbon dioxide, methane and volatile organic compounds, J. Anal. At. Spectrom., 39, 1444-1453, https://doi.org/10.1039/D3JA00330B, 2024.
Werle, P., Mücke, R., and Slemr, F.: The limits of signal averaging in atmospheric trace-gas monitoring by tunable diode-laser absorption spectroscopy (TDLAS), Appl. Phys. B, 57, 131-139, 1993.
Werner, R. A. and Brand, W. A.: Referencing strategies and techniques in stable isotope ratio analysis, Rapid Commun. Mass Spectrom., 15, 501-519, https://doi.org/10.1002/rcm.258, 2001.
Wojdyr, M.: Fityk: a general-purpose peak fitting program, J. Appl. Crystallogr., 43, 1126-1128, https://doi.org/10.1107/S0021889810030499, 2010.
Yu, L., Harris, E., Lewicka-Szczebak, D., Barthel, M., Blomberg, M. R. A., Harris, S. J., Johnson, M. S., Lehmann, M. F., Liisberg, J., Muller, C., Ostrom, N. E., Six, J., Toyoda, S., Yoshida, N., and Mohn, J.: What can we learn from N(2) O isotope data? - Analytics, processes and modelling, Rapid Commun. Mass Spectrom., 34, e8858, https://doi.org/10.1002/rcm.8858, 2020.